INVESTIGATIONS OF MHD ACTIVITY IN ASDEX DISCHARGES

R. Stambaugh[+], J. Gernhardt, O. Klüber, F. Wagner
and the ASDEX group

IPP III/103 June 1984

MAX-PLANCK-INSTITUT FÜR PLASMAPHYSIK

8046 GARCHING BEI MÜNCHEN

MAX-PLANCK-INSTITUT FÜR PLASMAPHYSIK

GARCHING BEI MÜNCHEN

INVESTIGATIONS OF MHD ACTIVITY IN ASDEX DISCHARGES

R. Stambaugh[+], J. Gernhardt, O. Klüber, F. Wagner
and the ASDEX group

IPP III/103 June 1984

Die nachstehende Arbeit wurde im Rahmen des Vertrages zwischen dem Max-Planck-Institut für Plasmaphysik und der Europäischen Atomgemeinschaft über die Zusammenarbeit auf dem Gebiete der Plasmaphysik durchgeführt.

IPP III/103

R. Stambaugh[+]
J. Gernhardt
O. Klüber
F. Wagner and the
ASDEX group

INVESTIGATIONS OF MHD ACTIVITY IN ASDEX DISCHARGES

ABSTRACT. This report records some specific observations of MHD activity in ASDEX discharges made in collaboration with J. Gernhardt, O. Klüber, and F. Wagner during the author's brief assignment at ASDEX in April, May, and June 1985. Because only a limited set of discharges were examined, no general conclusions about all of ASDEX data should be drawn. The discussion of the data makes a strong attempt to relate the ASDEX observations to observations made on the Doublet III and PDX tokamaks and to theoretical work on high ß MHD modes at GA and PPPL. Three topics are discussed.

The first topic is the detailed analysis of the time history of MHD activity in a ß limit discharge. The ß limit discharge in ASDEX is identified as a discharge in which, during constant neutral beam power, ß reaches a maximum and then decreases, often to a lower steady level if the heating pulse is long enough. During the L phase of this discharge, the MHD activity observed in the $\dot{B}$ coils is both a continuous and bursting coupled $m \geq 1$ mode of the "fishbone" type. When ß is rising in the H phase, this mode disappears; only ELMs are present. At $ß_{max}$, a different mode appears, the m = 2, n = 1 tearing mode, which grows rapidly as ß decreases.

The second topic is the very new observation of the fishbone-like mode in a discharge heated by combined neutral beam and ion cyclotron heating power. The mode characteristics are modulated by sawtooth oscillations in a manner consistent with the importance of q(0) in the stability of this mode.

The third topic is the search for ELM precursors in discharges designed to have no other competing and complicating MHD activity. In these cases non-axisymmetric precursors to the H_α spike were observed. Hence, it appears that an MHD mode, rather than an energy balance problem, must be the origin of the ELM.

[+]GA Technologies, San Diego, California

Section A

Analysis of MHD activity on shot 15520. A ß limit discharge

This discharge is ideal for exhibiting the variety of important MHD phenomena. It has sufficient $\dot{B}$ fluctuation data to make a complete time history of the modes. It has a steady L phase with both continuous and bursting modes dependent on the existence of the q = 1 surface in the plasma reminiscent of the fishbone mode. It has an L-H transition which quenches the fishbone type mode. At the ß peak the 2/1 mode becomes dominant and its growth may be what drives ß down. I offer the following time history of this shot. The shot had I = 320 kA, B_T = 2.17 T, B_p = 0.16 T, q_{OH} = 3.3, $q(ß_{Max})$ = 3.8, and 3.5 MW neutral injection power.

1.12 sec NBI comes on. The plasma is L mode. q(o) $\leq$ 1 as evidenced by sawteeth. The current profile begins to broaden. The last sawtooth is visible at 1.14 sec on the $\dot{B}$ traces in figure 1. The ECE profile estimated q(0) rises above 1 by 1.15 seconds but of course q(0) really lags the resistivity q(0) by the skin time ~ 100 msec so I have sketched the dashed q(0) curves in figure 1.

1.164 As $ß_p$ rises, $ß_p$ crosses the threshold (Ref. 1) for the instability of the fishbone-like mode. The mode grows to a saturated amplitude and is continuous and sinusoidal with no bursts. The $\dot{B}$ data obtained on this shot were the outer poloidal array of seven probes A1SSW, A4SSW, A6SSW, A7SSW, A8SSW, A10SSW, and A12SSW which span only 80.3° poloidally. The time delay of the peaks of the waveforms was plotted versus probe poloidal angle. A straight line was fit through these data by the method of least χ^2. The straight line fit was very good in all cases. The slope gave the phase advance in microseconds per degree of poloidal angle, from which one obtains the ratio m/n = (# µsec/deg.) x 360° x f (MHz). In this case, assuming the mode has n = 1, the m number is 2.8 ± 0.3. This type of m number is expected for the fishbone because as shown in Ref. 1, 2, this mode has a spectrum of m values from 0 to 5 but peaked between 2 and 3. The peak of the m number spectrum increases as $ß_p$ increases, an effect which may be seen in figure 1 (m increases to 3.5). Despite the m spectrum, a sinusoidal $\dot{B}$ trace is seen

because this mode is a kink distortion of the whole plasma column which does not form magnetic islands on rational surfaces (ref. 1). Another feature of the fishbone mode is that the mode has much smaller amplitude on the inside of the torus than on the outside (2). This in/out ratio is 0.58 → 0.36 → 0.5 in this shot. As will be seen later, the ordinary 2/1 tearing mode has a larger ratio. Figure 1 also shows a strong dependence of in/out ratio on plasma horizontal position so we must compare in/out ratios at the same horizontal position.

1.211 The continuous mode develops into bursts. These bursts have the same poloidal mode number as the continuous mode and the same frequency. Actually the frequency rises from 28.5 kHz to 43 kHz slowly and steadily from the continuous phase to the end of the bursts. We conclude the continuous mode and the bursting mode are the same mode, the fishbone-like mode discovered on PDX. The theory of the fishbone mode depends only on the pressure of trapped fast ions, in fact on the trapped fast ion poloidal ß (3). Because ASDEX has tangential injection and hence no trapped fast ions, the description of the burst cycle given in reference 3 cannot apply to ASDEX. It may apply to PDX, in which all the fast ions were trapped. Doublet III had an intermediate injection angle of 27^{o} off perpendicular and so had about equal populations of trapped and untrapped fast ions. We also saw both continuous fishbone type modes (as in the tangential injection machines ISX and ASDEX) with no associated fast ion loss and the bursting fishbone mode with associated fast ion loss. When we saw the fast loss, the mode amplitude $\Delta B/B$ was about 1 to 2 %. The amplitudes in ASDEX are much smaller (0.04 %) and no fast ion losses are observed so I believe this mode in ASDEX has no effect on the fast ions nor do the fast ions have any effect on the mode.

Why then does the mode burst? L. Chen and others at PPPL have called this mode an internal kink because it is much more unstable when q(0) is less than 1 and for the trivial reason that their calculations used a fixed plasma boundary. Lee at GA (1) called the mode an external kink because he put $q(0) > 1$ and

used a free boundary. But he used the same code, HIB developed at PPPL, and got basically the same modes as L. Chen. The only meaningful difference was in the amplitude of the m = 1 component of course. I think the PPPL view of this mode as an internal kink is more correct because it emphasizes the strong role of q(0). In Doublet III the fishbones turned off at the bottom of a sawtooth (q(0) ~ 1.1) and turned on near the top of the sawtooth (q(0) ~ 0.9). I believe such a dependence on sawtooth phase and hence q(0) was seen in PDX (and ASDEX? See section B). So in shot 15520 I believe the axial q is about 1.0 during the time of the bursts and its slight modulation causes the bursts. Lee (1) showed that the growth rate of the mode $\alpha\beta_p^5$. This strong dependence means that β_p also acts like a switch between stable and quickly non-linearly saturated states. So some interaction of the values of q(0) and β_p may produce the bursts.

1.268 The bursts stop and H_α starts to rise. After the last burst the same mode may be present but the frequency would be 10 kHz. Some double frequency features are seen so we may have m = 1 and m = 2.

1.271 The L → H transition occurs. H_α drops. ß rises faster. The plasma moves out. The MHD activity is non-existent. An upper limit is $\Delta B/B \sim 0.02$ % at 10 kHz.

1.31 The first and largest ELM occurs and the rate of increase of ß becomes smaller. The axial q is estimated from ECE to be rising. We may attribute the absence of the fishbone mode to q(0) > 1.

1.35 ß is maximum. A burst larger than usual for an ELM appeared. Between most ELMs at this time, the same mode as in the large burst is present but goes up and down in amplitude and shows some bursts. The frequency is 41 kHz. The poloidal phase pattern is similar to the fishbone. The phase delay from probe A4 to A12 (58.4^o poloidally) is 12 μsec → m/n = 3.1. The in/out ratio is 0.57 and $\Delta B/B = 0.016$ %. This mode may be the fishbone trying to reappear at q(0) > 1 but at higher β_p.

1.365 The MHD activity suddenly increases and ß starts to decrease. More than one mode is present. The low frequency mode is 15.5 kHz. The in/out ratio is 1.24 at the same radial position as the fishbone earlier in the shot. $\Delta B/B$ is 0.06 %. Another mode is present with a higher frequency and lower amplitude. The two modes do not seem to have a fixed phase relation to each other, which makes the m/n number determination difficult. Occasionally, the second mode goes away for one or two cycles of the larger mode. During such a period, $m/n = 2.6 \pm 0.4$ was measured for the larger mode. The smaller mode could not be identified.

1.3815 to 1.420 The two frequency feature disappears. A clear sinusoidal mode is left. The m/n value is 2.0 throughout the ß decrease. In these cases, about a 6 % increase in m/n was applied to correct for about 2.5 cm of inward motion of the plasma. The frequency decreases from 16.3 kHz to 10 kHz. The amplitude $\Delta B/B$ measured on the outside of the torus rises from 0.06 % to 0.24 % despite a strong inward motion. So 0.24 % underestimates the amplitude. The amplitude on the inside wall reaches 0.6 %. The in/out ratio is much higher than for the fishbone but the largest values have a lot to do with the inward plasma motion. The neutral beam turns off about 1.415 sec. The ß fall seems clearly correlated with the growth of the m = 2, n = 1 tearing mode. H_α in the dome (fig. 2) rises but H_α in the main chamber has only a small rise at 1.40 sec. This tearing mode is distinguished from the fishbone by its m/n = 2 value, by its lower frequency, and by its in/out amplitude ratio, and by its larger absolute amplitude.

Section B

MHD activity in a combined neutral beam and ICRF heated discharge

Combined NI and ICRF heated discharges yield $\dot{B}$ fluctuation data which exhibits very standard fishbone mode features as seen in Doublet III (ref. 2). In particular the modulation of the mode activity by the sawtooth is clearly evident. We present here the mode analysis of shot 16185. This

discharge had I_p = 370 kA at B_T = 2.17 T and q ~ 3.1. It was heated with 7 Neutral Beam Sources at about 3.05 MW and also 2 MW of ICRH power. This discharge never goes into the H mode but is well heated. The 8 source shot 15520 reached β_T = 0.5% in the L mode; this discharge reaches β_T = 0.65 %. The increased β_T may be accounted for by the higher current (370 kA/320 kA = 1.16) and by the higher power (5 MW/3.5 MW = 1.43) for a combined ratio of 1.66. The β_T ratio is 0.65/0.5 = 1.3.

Traces for shot 16185 are shown in figure 3. The plasma is displaced outward by about 3 cm to R = 168 cm from the "normal" ASDEX position of R = 165 cm. The vertical position is low, indicating lower single null operation. The density is about 4 x 10^{13} cm^{-3} and the density trace clearly shows the sawteeth. Late in the heating phase the sawteeth become especially large in the divertor H_α (trace 7) and can be seen in the diamagnetic loop β_T signal. An inset of the Mirnov loop signals is placed in the figure above the density trace. The $\dot{B}$ activity is clearly correlated with the sawtooth in the manner described in section A of this report. Just after a sawtooth fall, when q(0) is just above 1, the $\dot{B}$ activity is zero. As the sawtooth rises, and presumably q(0) becomes equal to 1.0, bursts appear, which may be the fishbone mode turning on and off as q(0) is modulated around 1.0. Near the top of the sawtooth; as q(0) becomes always less than 1.0, the bursts go into a continuous mode. When the sawtooth fall occurs, this mode is completely switched off. This cycle repeats.

Sufficient data were obtained from the paper outputs and were captured in the computer to identify this mode. From the paper outputs, by measuring phase delays among three toroidally displaced probes (A8 NNW, A8 WNW, A8 SSW) the calculated toroidal mode number was 1.13 $\pm$ 0.06 or n = 1. The computer captured the outer poloidal probes (A7 SSW, A6 SSW, A9 SSW, A12 SSW, A15 SSW) and (I2 SSW, I5 SSW, and I8 SSW) on the inside. An expansion of the data on probe A9 SSW is shown in figure 4.

The inside probes have no observable signal, which is consistent with the nearly zero inside amplitude found for the fishbone on Doublet III. In this case, however, the outward shift of the plasma must play a large part in suppressing the inside signal. The m/n number (or m since n = 1) was measured by χ^2 fitting a straight line to the phase delays on the outer probes as a function of poloidal angle. The results are summarized in table 1.

Table 1

Time (sec)	mode	f (kHz)	m/n	ΔB/B (out) (%)
1.231	Burst 1	23.8	3.49 ± .3	0.023
1.233	Burst 2	21.6	3.42 ± .24	0.037
1.235	Burst 3	20.0	3.35 ± .22	0.068
1.237	Burst 4	21.0	3.68 ± .23	0.081
1.239	Burst 5	20.4	3.66 ± .23	0.12
1.241	Burst 6	19.5	3.54 ± .22	0.11
1.244	Burst 7	19.0	3.47 ± .21	0.092
1.248	Continuous	18.5	3.53 ± .21	0.086
1.257	Continuous	17.4	3.32 ± .2	0.12

Because of the slow variations in frequency, mode number, and amplitude, we conclude the bursting mode and the continuous mode are the same mode, the fishbone mode.

Section C

Search for ELM Precursors

The following discharges were examined closely for evidence in the $\dot{B}$ signals of a precursor to an ELM: Shots 15705, 15756, 15757, 15764, 15768, 15771, 15773, 15814. These discharges were selected and designed for no competing MHD activity during the ELM period. Because one expects the ELM precursor to show only one or two cycles prior to the H_α burst, any other mode that is present makes the identification of the ELM precursor impossible. The data are of lesser quality on shots 15705, 15768, and 15771 and will not be presented.

The most important conclusion is that a non-axisymmetric precursor does exist up to 50 microseconds before any perceptible increase in H_α in the main chamber. A possible delay in the H_α signal with respect to the $\dot{B}$ signals was separately tested. In response to a steep increase in light on the photodiode, the signal starts

to rise in less than one microsecond but rolls up as if charging a capacitively loaded circuit with a time constant of 8 microseconds. Hence the H_α emission rises somewhat faster than the signal traces in this report, but the start time is accurate and what is called a precursor in this report is indeed a precursor. The fact that the precursor is non-axisymmetric seems to rule out models of the ELM which depend on energy balance collapse in the plasma edge, at the X-point, or in the divertor channel. An MHD mode for the cause of the ELM is favored.

The data taken were on the mainly toroidal distribution of probes.

Probe	Poloidal angle	Toroidal angle
ES 1 (NO)	0.0	302.5
A8 (NNW)	0.0	12.0
A8 (WNW)	0.0	74.0
ES4 (W)	0.0	102.0
ES3 (SW)	0.0	128.5
A8 (SSW)	0.0	168.0
I8 (SSW)	158.1	168.0
I5 (SSW)	180.0	168.0

A toroidal distribution was chosen in order to try to distinguish between ballooning and kink/tearing modes on the basis of the toroidal mode number n. The argument is that n = 1 modes may be either kink or ballooning modes. But modes with $n \geq 3$ are probably ballooning modes because ballooning modes are most unstable for $n = \infty$ and most stable for n = 1 so their n numbers appear from above. For tearing modes, the lowest order mode is most unstable, so one always expects to see n = 1 before n = 3. Lackner argues, however that, neglecting the effect of the X point on q only certain rational surfacs exist where $\vec{\nabla}J$ is high, so that it is possible to have higher n number tearing modes appear before n = 1.

Precursors with n = 1 are often seen. They generally come late in the H-phase and often precede a transition back to the L phase, or a disruption, or in general some event after which the H_α level below the ELMs remains high. An example is shot 15756 (figs. 5, 6). A precursor of low n, $0 \leq n \leq 1$, is seen 40 sec ahead of the last H_α rise. One msec after this H

rise is a major disruption. Shot 15764, expansion B1, fig. 13 shows an ELM preceeded for 50 μsec by a precursor adequately described by n = 1. Only perhaps a 1/4 cycle is seen or else the mode is purely growing. A period of high background H_α follows this ELM, which is the last clear ELM (see figure 11).

Shot 15814 (fig. 23) has the unusual feature of having perhaps 3/4 of a cycle before the ELM. The magnetic pattern is sufficiently detailed that the disturbance can be tracked as it propagates from 168^o to 74^o to 12^o. Phase shifts were measured and with an estimate of the frequency of 8.7 kHz, n = 1 was calculated. The estimated amplitude of the disturbance is 1.2 G or $\Delta B/B = 0.09$ %. The poloidal mode number m is in general hard to determine on ELM precursors because the precursor is very weakly seen on the inside major radius of the torus.

There is some evidence for precursors with n > 2. In shot 15764, ELM A (fig. 12) and ELM B2 (fig. 14) may be n = 3 or even 6. In fig. 12, the probes at 302.5^o and 12.0^o (70^o between) have opposite signals so n ~ 3. The probes at 12^o and 74^o (62^o between) have opposite signals so n ~ 3. The probes at 102^o and 168^o (66^o between) have opposite signals so n ~ 3. In figure 14 these pairs of probes have opposite signals: (302.5^o, 12^o, 70^o between), (12^o, 74^o, 62^o between), (168^o, 102^o, 66^o between) implying n ~ 3. These probe pairs have similar signals: (74^o, 102^o, 28^o between) and ($128,5^o$, 168^o, 30^o between) which could be consistent with n ~ 3.

A progression of four ELMs is seen in shot 15773 (figs. 15-22). The series of ELMs (fig. 16) leads up to a period of high H_α. The first ELM (B3, fig. 21) has a very weak precursor. The second ELM (B1, fig. 22) has a visible precursor for 30 μsec. An adequate description is n = 1. There s ringing of a mode after the ELM and this ringing has n = 1. The third ELM (B4, fig. 19) has a 25 μsec precursor that is well described by n = 1 and the ringing after the ELM is also $n = 1 \pm 0.3$ at 7 kHz. The fourth ELM (B2, fig. 20) is well described as n = 1 and after this ELM, the H_α level remains high.

Shot 15757 (figs. 7, 8, 9) is included to give a balanced view. There are no visible precursors in this shot.

To summarize, then, nonaxisymmetric ELM precursors are seen for up to 50 sec before the H_α increase. These precursors are usually n = 1. ELMs that are late in the discharge are n = 1 and of sufficiently strong amplitude to be clearly identified. Irreversible transitions to high H_α states are preceeded by an ELM with an n = 1 precursor. There is some evidence for n > 2 precursors. ELMs that occur early in the H phase tend to have weak, hard to identify precursors. The n > 2 cases are early ELMs. The precursor is rarely visible at all on the inside wall of the torus; only the outside probes show the ELM precursor clearly.

Acknowledgement

I would like to thank all the members of the ASDEX team for helping to make my short stay a productive one.

References

/1/ J.K. Lee, M.S. Chu, F.J. Helton, and W. Park, Europhysics Conference Abstracts, Ed. S. Methfessel, 11th Europ. Conf. on Controlled Fusion and Plasma Physics, Aachen 1983, Vol. 7D, part, II, p. 231

/2/ E.J. Strait, L.C. Bernard, J.K. Lee, R.W. Moore, R.D. Stambaugh and Doublet III Physics, Europhysics Conference Abstracts, Ed. S. Methfessel, 11th Europ. Conf. on Controlled Fusion and Plasma Physics, Aachen 1983, Vol. 7D, part, I, p. 59

/3/ L. Chen, R.B. White, C.Z. Cheng, F. Romanelli, J. Weiland, R. Hay, J.W. Van Dam, M.N. Rosenbluth, S.T. Tsai, D.C. Barnes, Plasma Physics and Controlled Nuclear Fusion Research 1984, Tenth Conf. Procs., London, Sept. 1984, Nuclear Fusion, Supplement 1985, Vol. 2, IAEA-CN-44/E-II-1

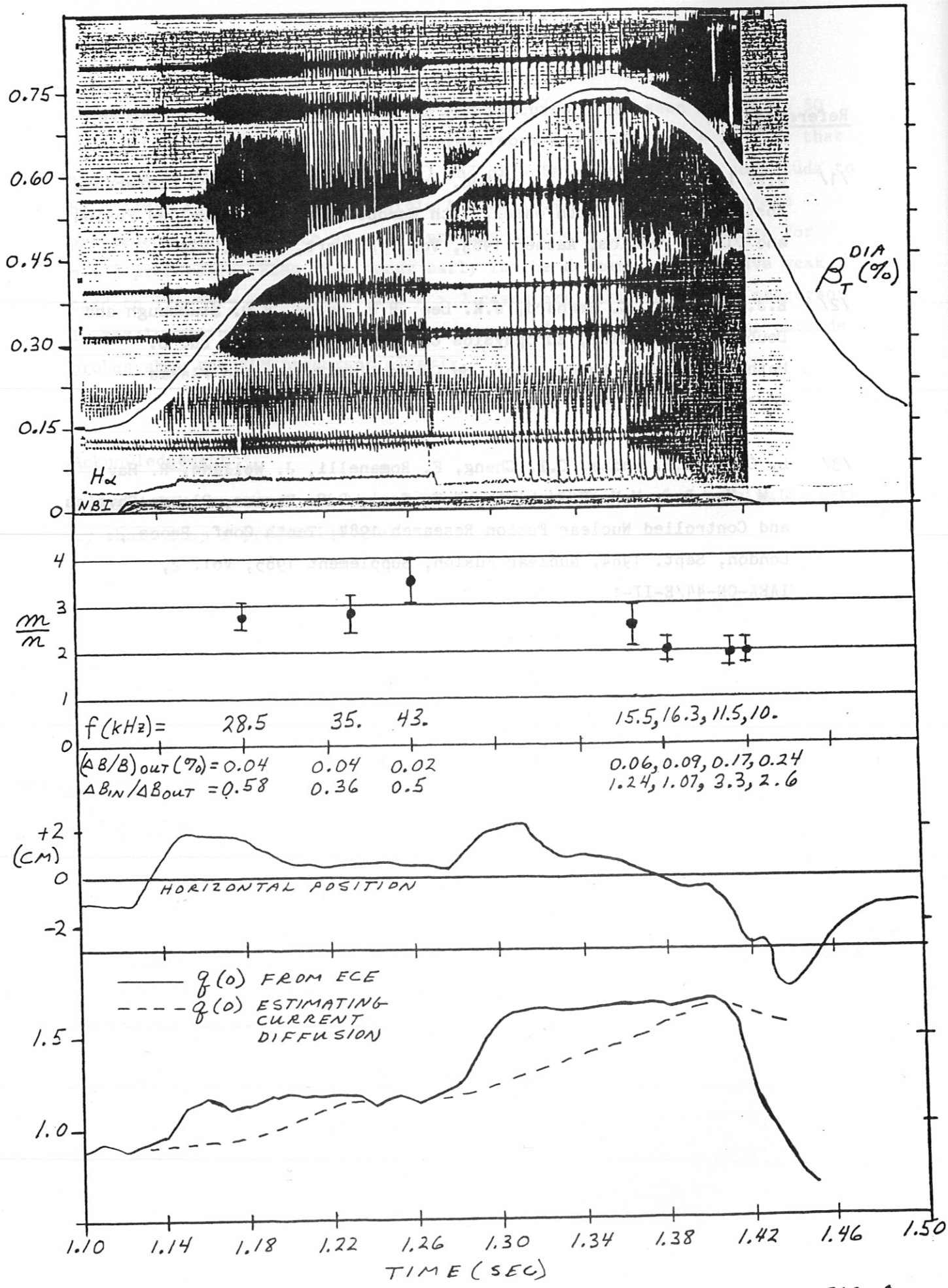

SHOT 15520

FIG. 1

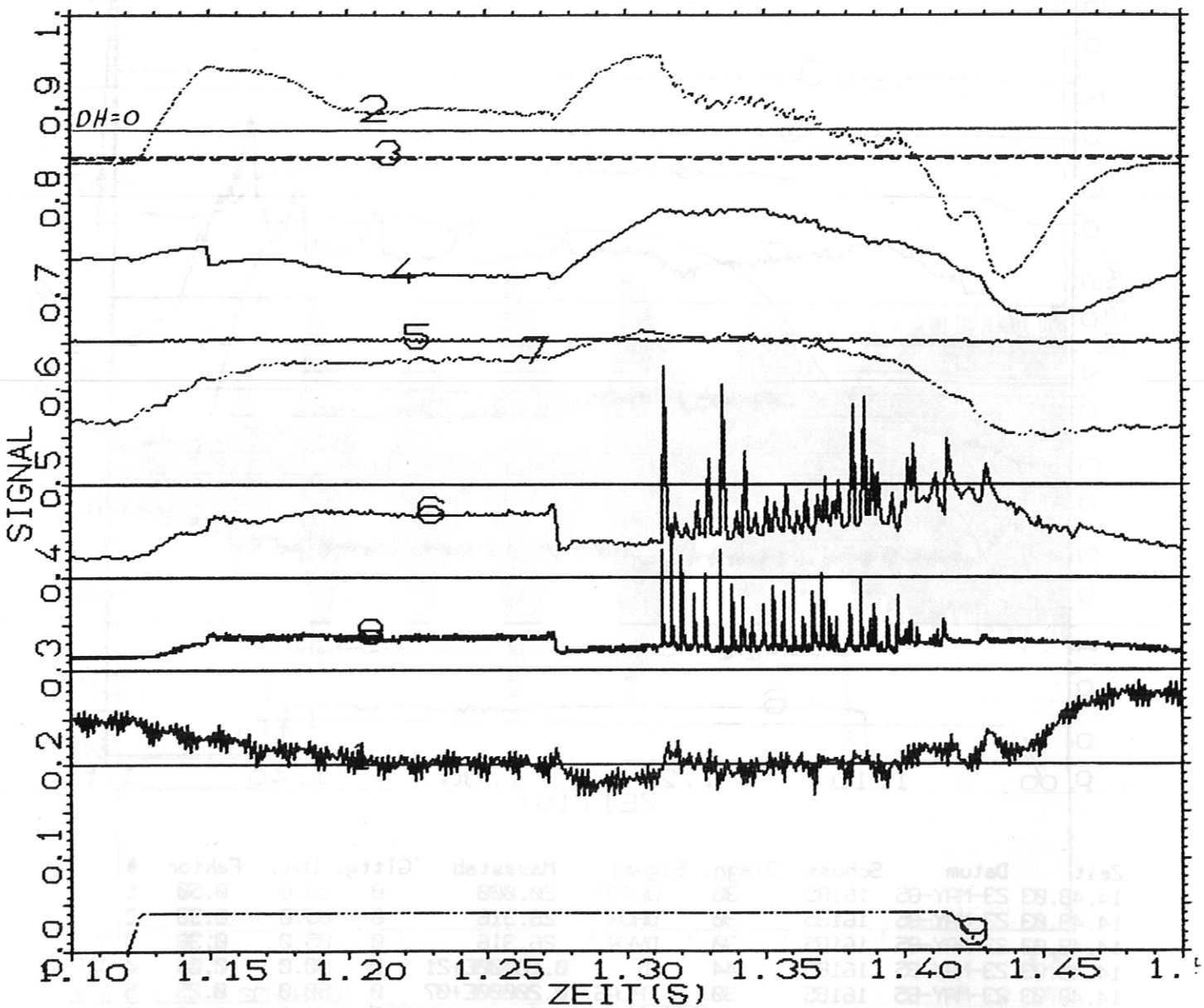

Zeit	Datum	Schuss	Diagn.	Signal	Massstab	Gl	ttg.	Unt.	Faktor	#
10.24.46	23-APR-85	15520	30	ULOOP	20.000	0		20.0	0.50	1
10.24.46	23-APR-85	15520	30	DHOR	26.316	0		85.0	0.38	2
10.24.46	23-APR-85	15520	30	DVER	26.316	0		85.0	0.38	3
10.24.46	23-APR-85	15520	44	H1	0.10000E+21	0		50.0	0.84	4
10.24.46	23-APR-85	15520	30	JPLAS	0.20000E+07	0		50.0	0.25	5
10.24.46	23-APR-85	15520	31	FDKO	10.000	0		40.0	0.50	6
10.24.46	23-APR-85	15520	3	VFI	485.06	0		40.0	0.40	7
10.24.46	23-APR-85	15520	32	FDASOT	0.19531E-01	0		30.0	1.00	8
10.24.46	23-APR-85	15520	31	NI	100.00	0		0.0	0.05	9

FIG. 2

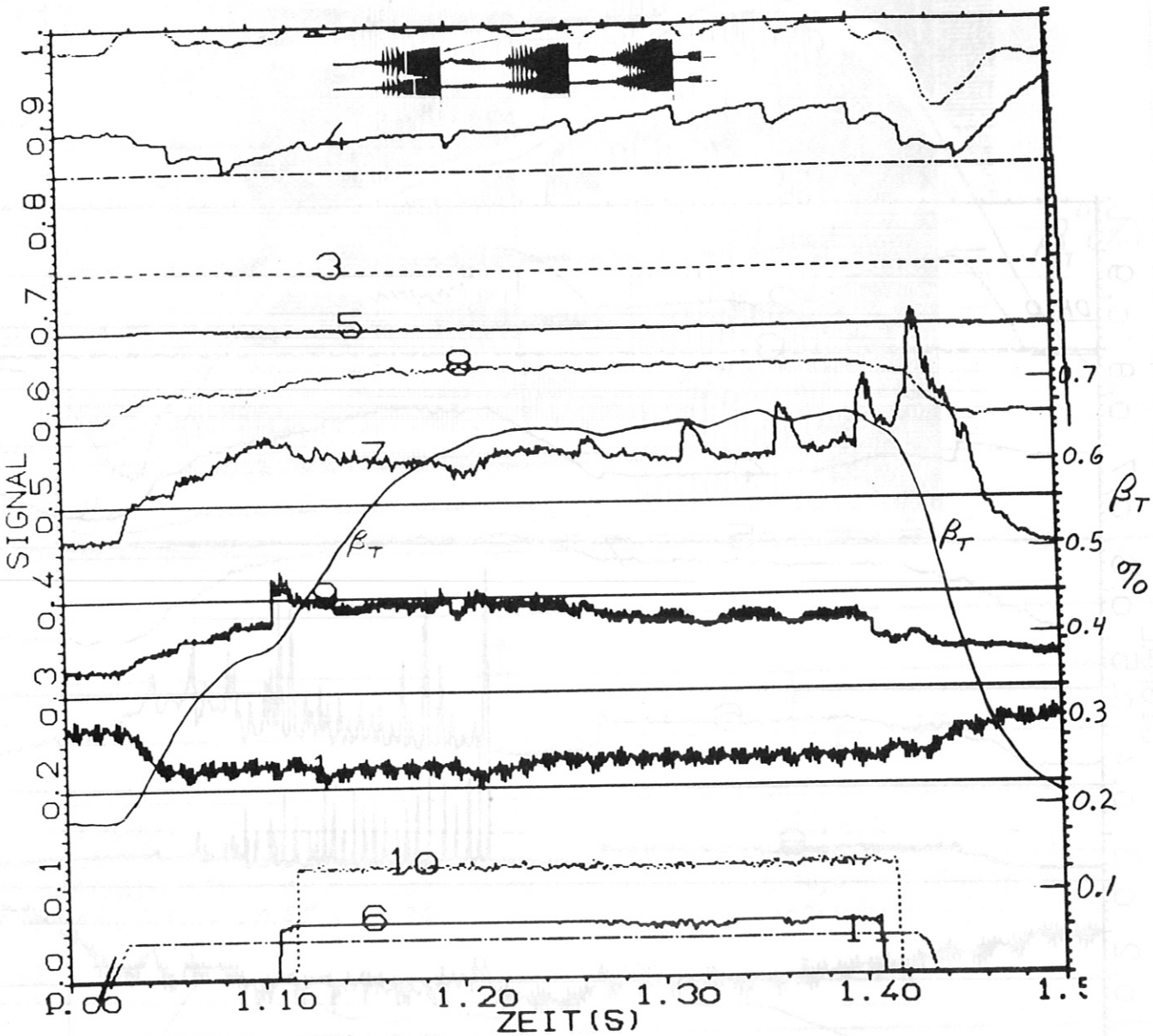

Zeit	Datum	Schuss	Diagn.	Signal	Massstab	Gltg.	Unt.	Faktor	#
14.48.03	23-MAY-85	16185	30	ULOOP	20.000	0	20.0	0.50	1
14.48.03	23-MAY-85	16185	30	DHOR	26.316	0	85.0	0.38	2
14.48.03	23-MAY-85	16185	30	DVER	26.316	0	85.0	0.38	3
14.48.03	23-MAY-85	16185	44	H1	0.10000E+21	0	50.0	0.84	4
14.48.03	23-MAY-85	16185	30	JPLAS	0.20000E+07	0	50.0	0.25	5
14.48.03	23-MAY-85	16185	30	ICRH1	50.000	0	0.1	0.10	6
14.48.03	23-MAY-85	16185	31	FDKO	10.000	0	40.0	0.50	7
14.48.03	23-MAY-85	16185	3	VFI	485.06	0	40.0	0.40	8
14.48.03	23-MAY-85	16185	32	FDASOT	0.19531E-01	0	30.0	1.00	9
14.48.03	23-MAY-85	16185	30	ICRH2	33.333	0	0.1	0.15	10
14.48.03	23-MAY-85	16185	31	NI	100.00	0	0.0	0.05	11

FIG. 3

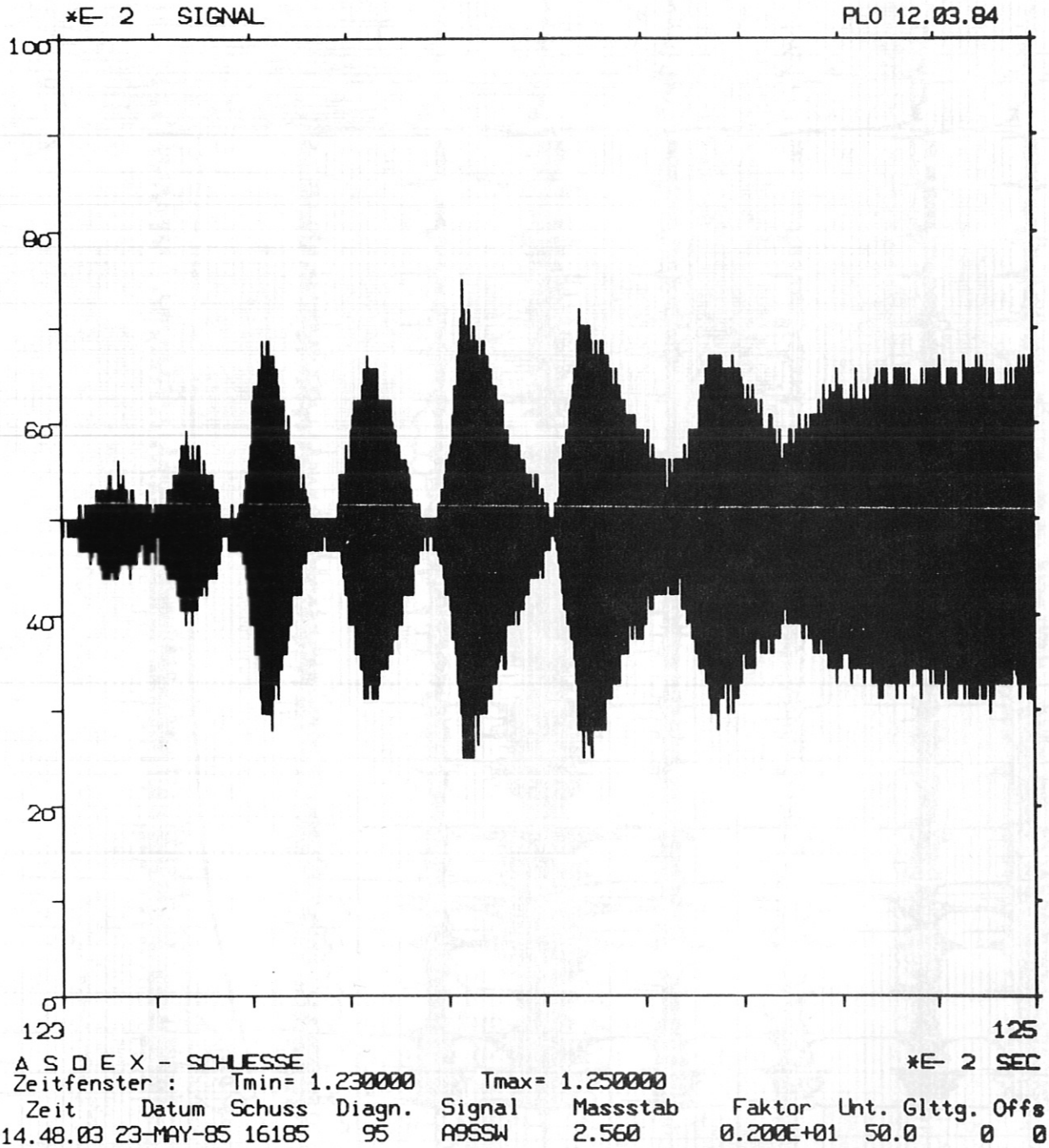
*E- 2 SIGNAL
PLO 12.03.84
100
80
60
40
20
0
123
125
A S D E X - SCHUESSE
*E- 2 SEC
Zeitfenster : Tmin= 1.230000 Tmax= 1.250000
Zeit Datum Schuss Diagn. Signal Massstab Faktor Unt. Glttg. Offs
14.48.03 23-MAY-85 16185 95 A9SSW 2.560 0.200E+01 50.0 0 0

FIG 4

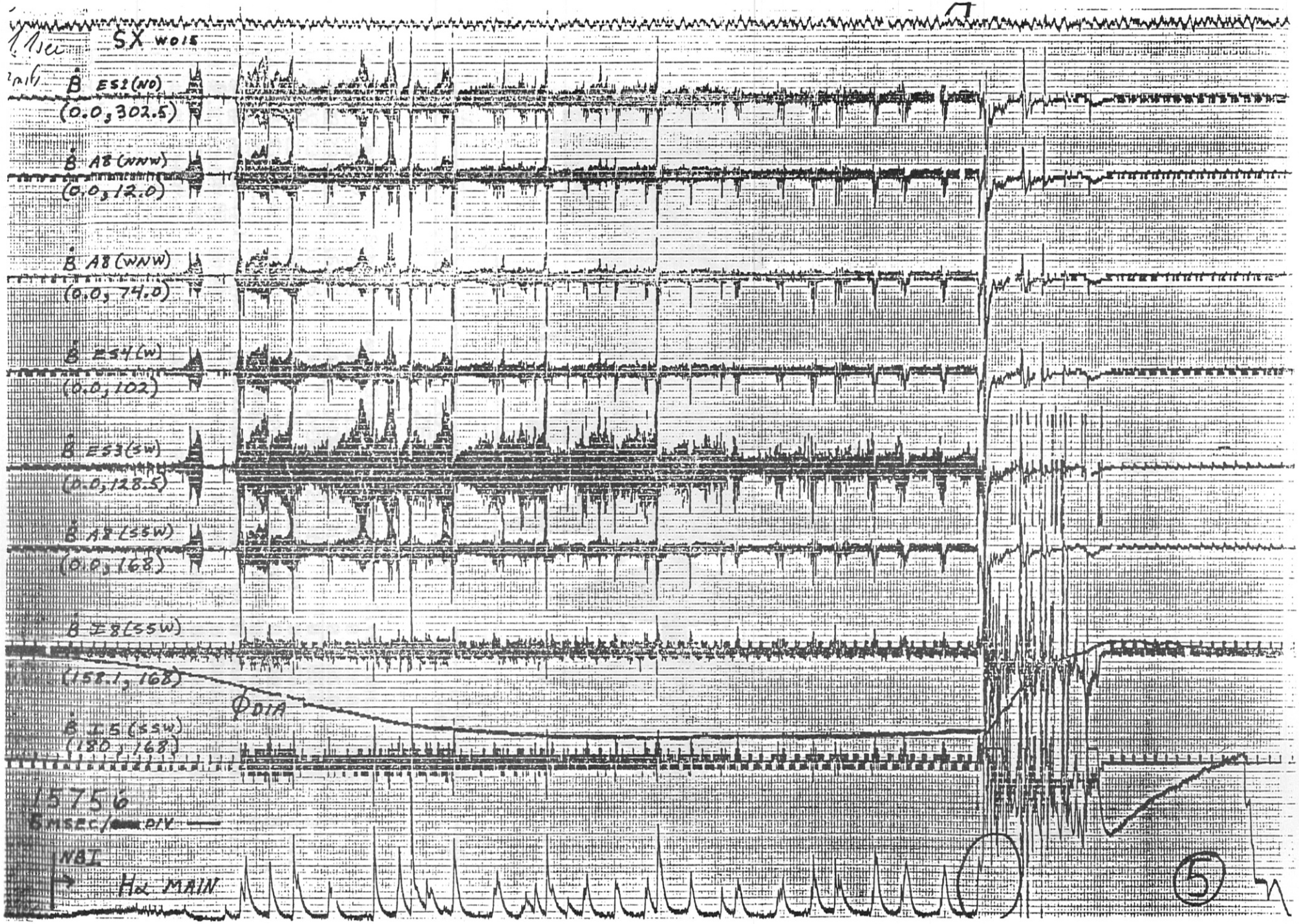
SX W015
Ḃ ES2(NO)
(0.0, 302.5)
Ḃ A8 (WNW)
(0.0, 12.0)
Ḃ A8 (WNW)
(0.0, 74.0)
Ḃ ES4 (W)
(0.0, 102)
Ḃ ES3 (SW)
(0.0, 128.5)
Ḃ A2 (SSW)
(0.0, 168)
Ḃ I8 (SSW)
(158.1, 168)
ΦDIA
Ḃ I5 (SSW)
(180, 168)
1576
5 msec/ DIV
NBI
Hα MAIN
①
⑤

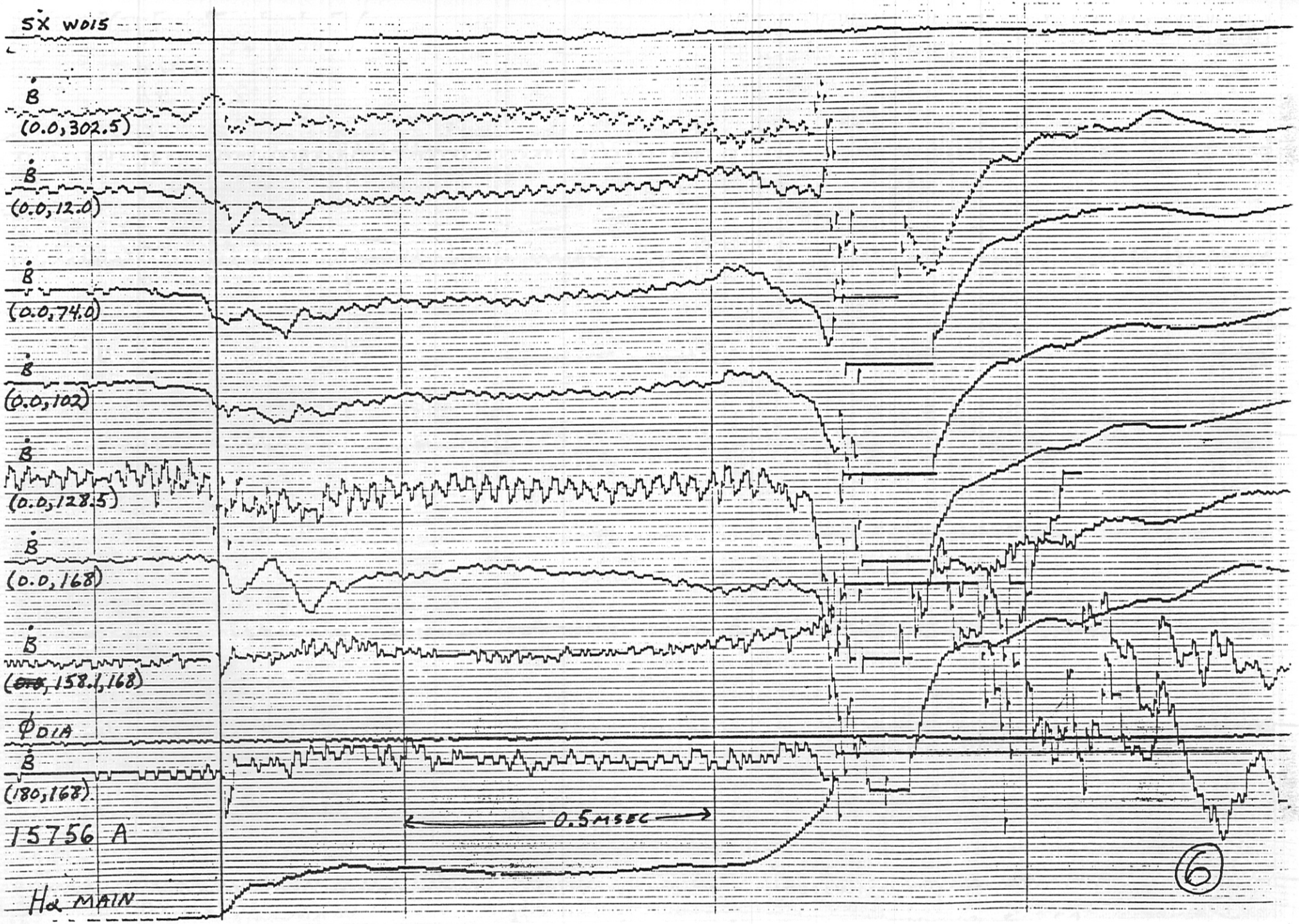
SX W015
Ḃ
(0.0, 302.5)
Ḃ
(0.0, 12.0)
Ḃ
(0.0, 74.0)
Ḃ
(0.0, 102)
Ḃ
(0.0, 128.5)
Ḃ
(0.0, 168)
Ḃ
(~~0.0~~, 158.1, 168)
ϕ DIA
Ḃ
(180, 168)
0.5 MSEC
15756 A
Hα MAIN
6

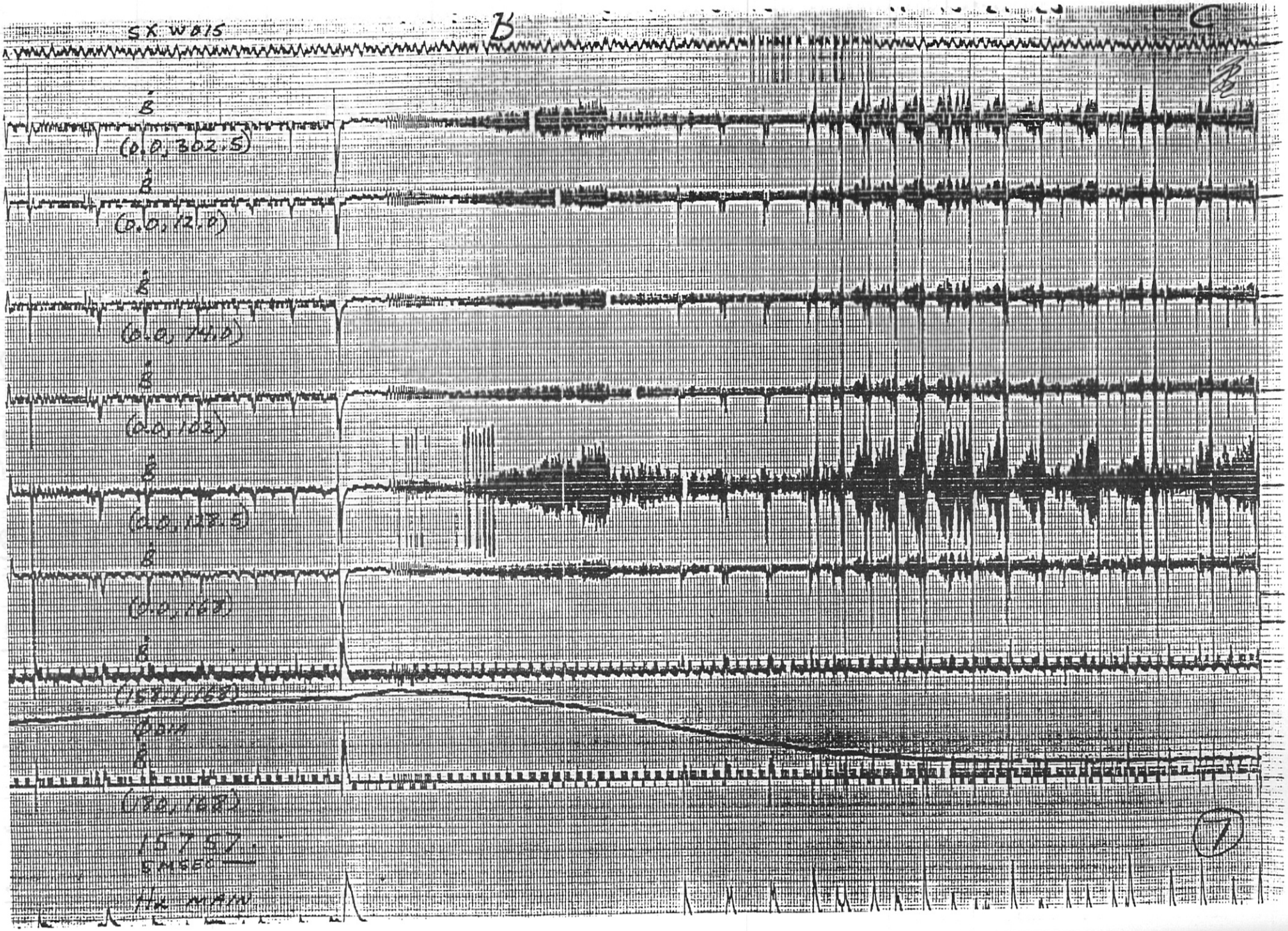
SX W815
B
C
B
B
(0.0, 302.5)
B
(0.0, 12.0)
B
(0.0, 74.0)
B
(0.0, 102)
B
(0.0, 132.5)
B
(0.0, 162)
B
(157.5, 188)
POW
B
(180, 188)
1575
5 MSEC
Hz MAIN
D

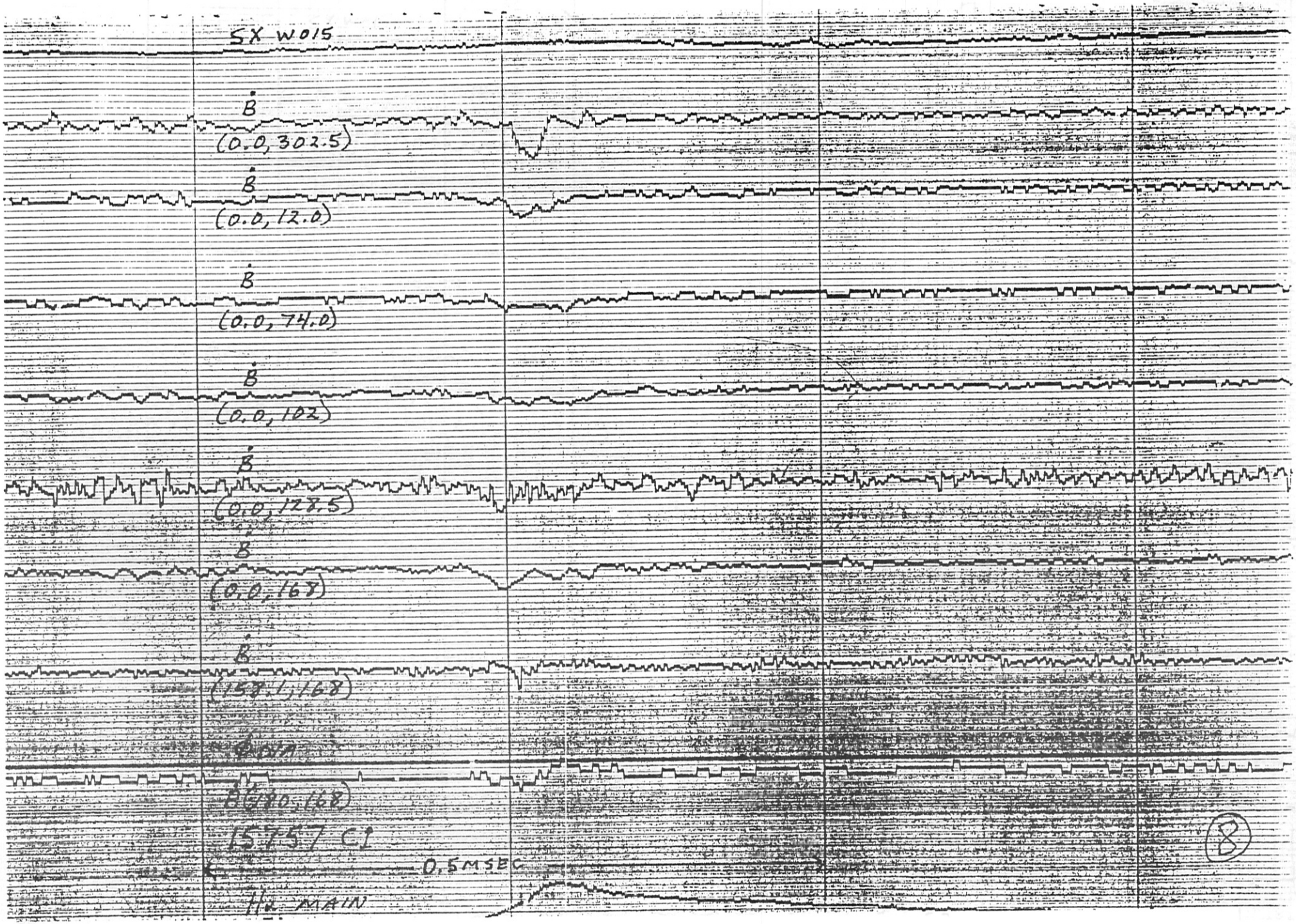
SX W015
$\dot{B}$
(0.0, 302.5)
$\dot{B}$
(0.0, 12.0)
$\dot{B}$
(0.0, 74.0)
$\dot{B}$
(0.0, 102)
$\dot{B}$
(0.0, 128.5)
$\dot{B}$
(0.0, 168)
$\dot{B}$
(153.1, 168)
$\dot{B}$(80.168)
[5757] C1
0.5MSEC
Ha MAIN
8

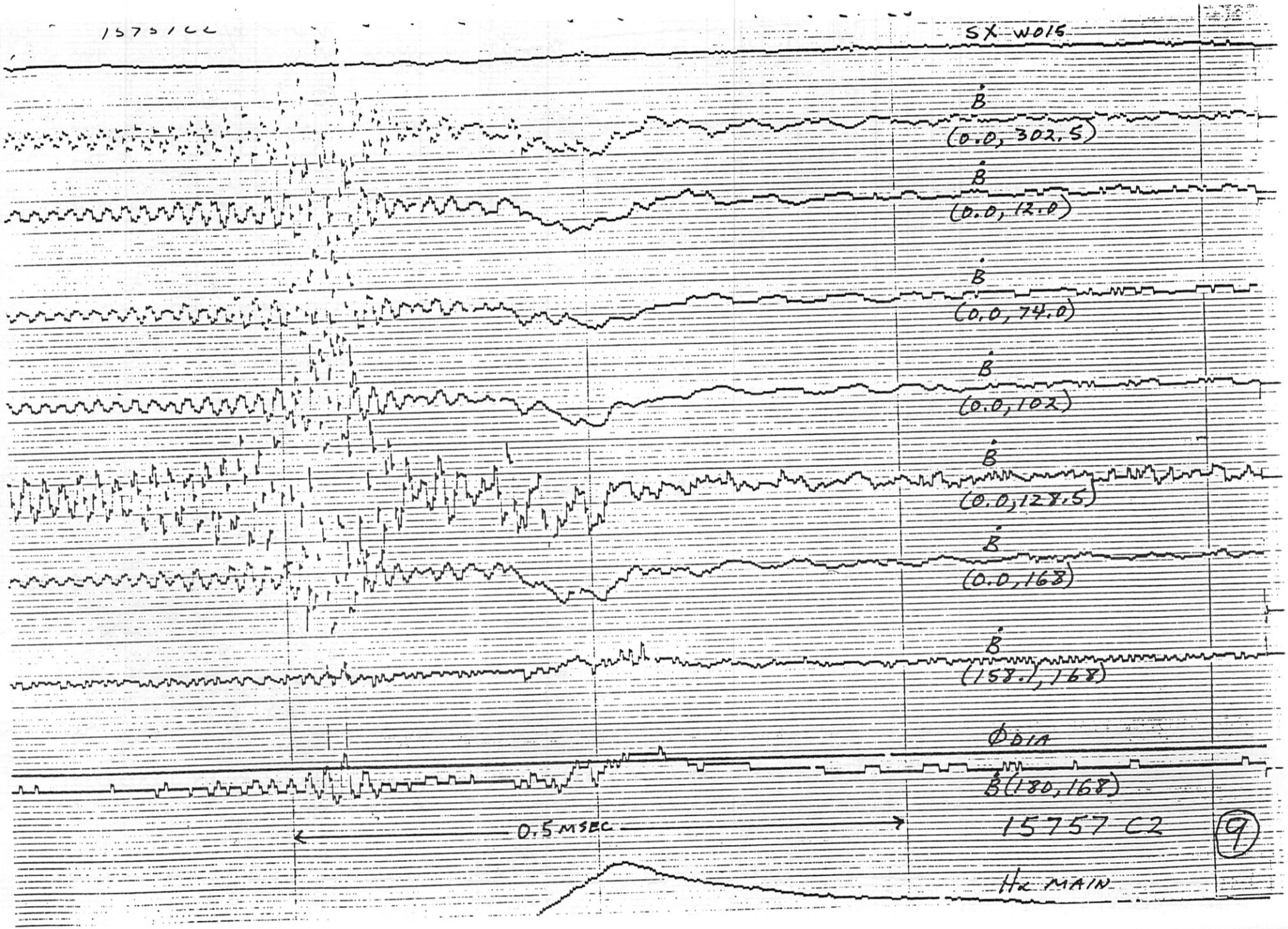
15751CC
SX W015
$\dot{B}$
(0.0, 302.5)
$\dot{B}$
(0.0, 12.0)
$\dot{B}$
(0.0, 74.0)
$\dot{B}$
(0.0, 102)
$\dot{B}$
(0.0, 127.5)
$\dot{B}$
(0.0, 168)
$\dot{B}$
(158., 168)
ϕ_{DIA}
$\dot{B}$(180, 168)
0.5 MSEC
15757 C2
9
Hz MAIN

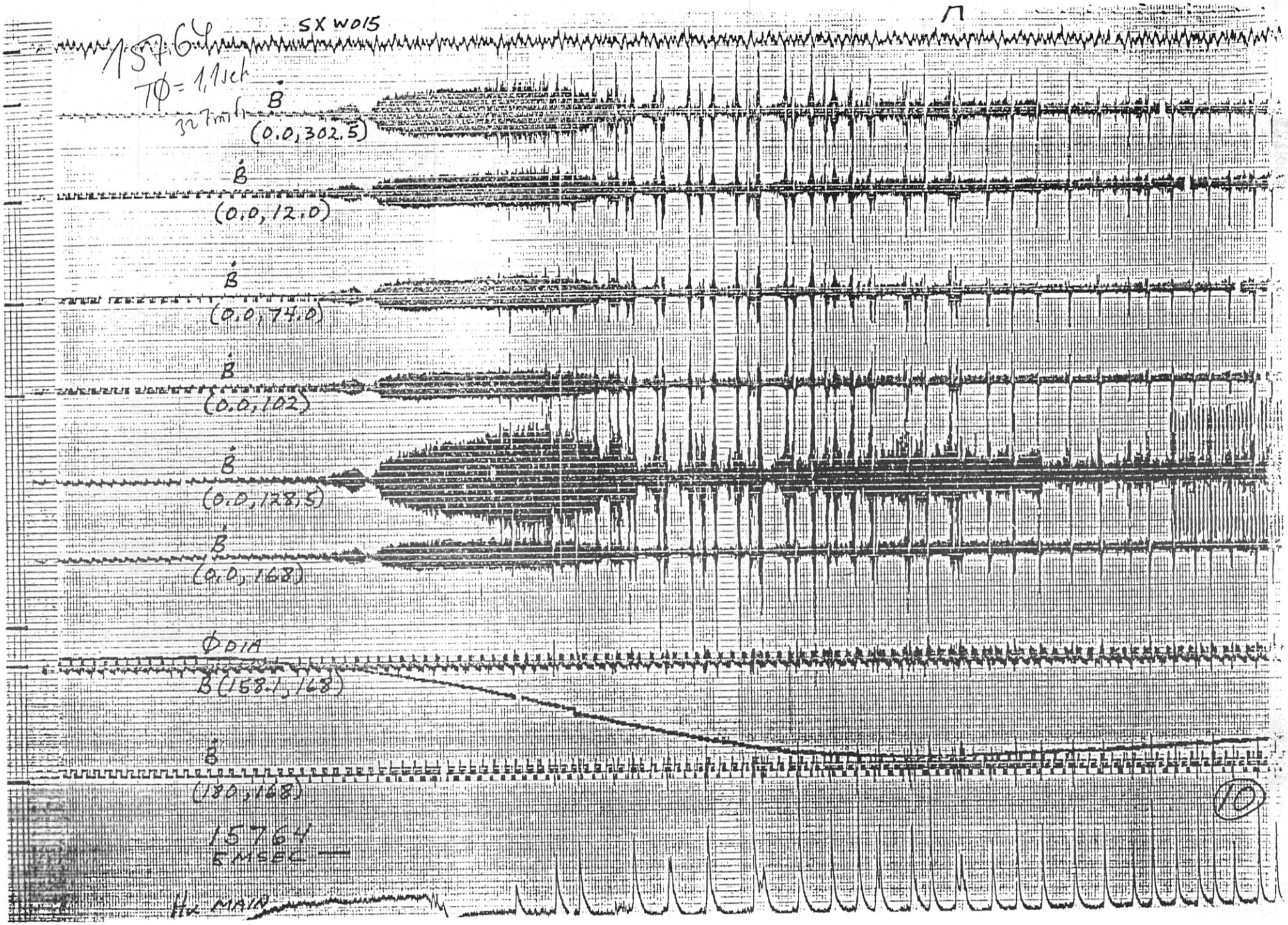
SX W015
TΦ = 1,1sec
Ḃ
(0.0, 302.5)
Ḃ
(0.0, 12.0)
Ḃ
(0.0, 74.0)
Ḃ
(0.0, 102)
Ḃ
(0.0, 128.5)
Ḃ
(0.0, 168)
ΦDIA
B (158.1, 168)
Ḃ
(180, 168)
15764
5 MSEC
Hz MAIN
10

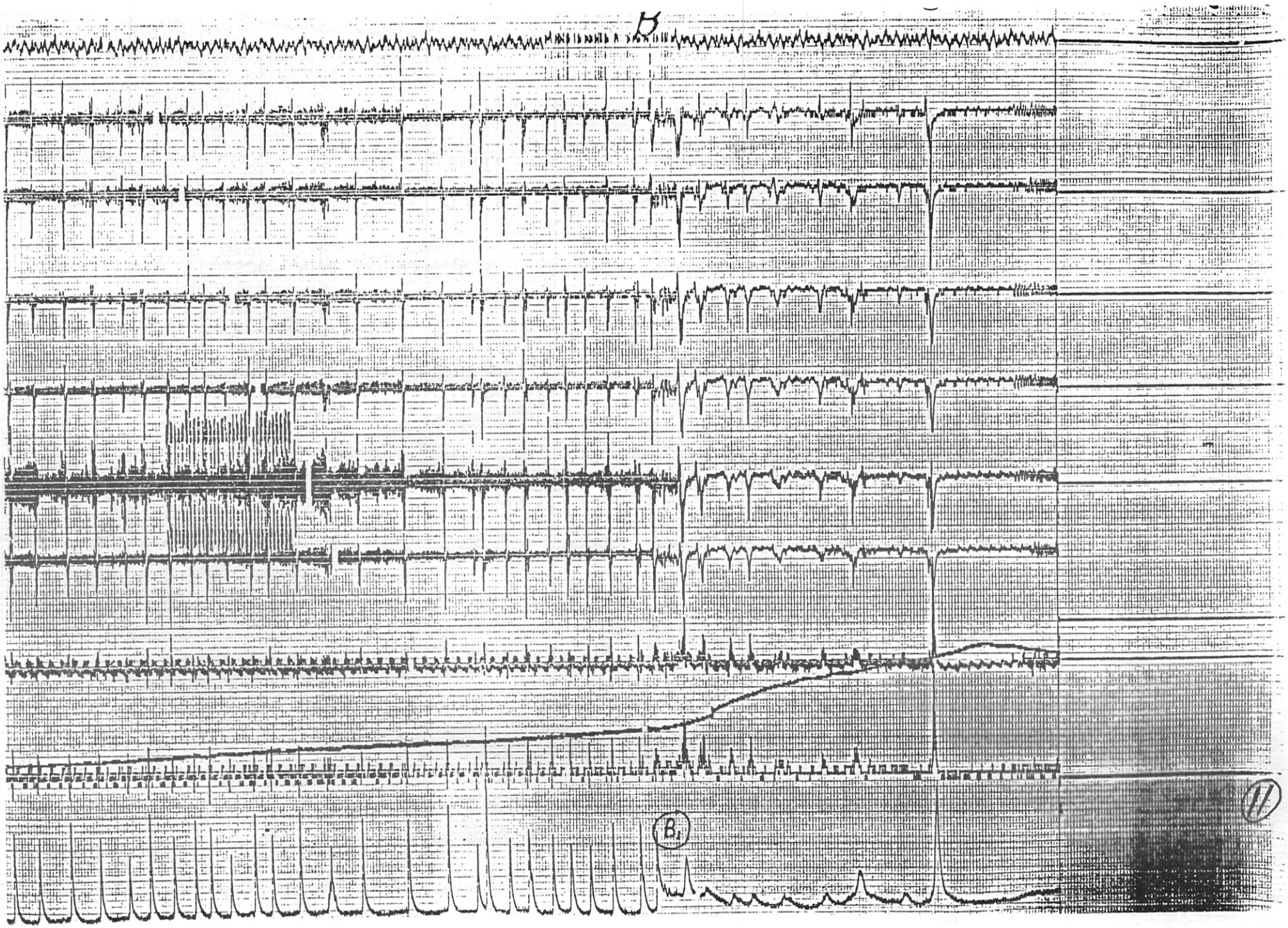
B
B1
II

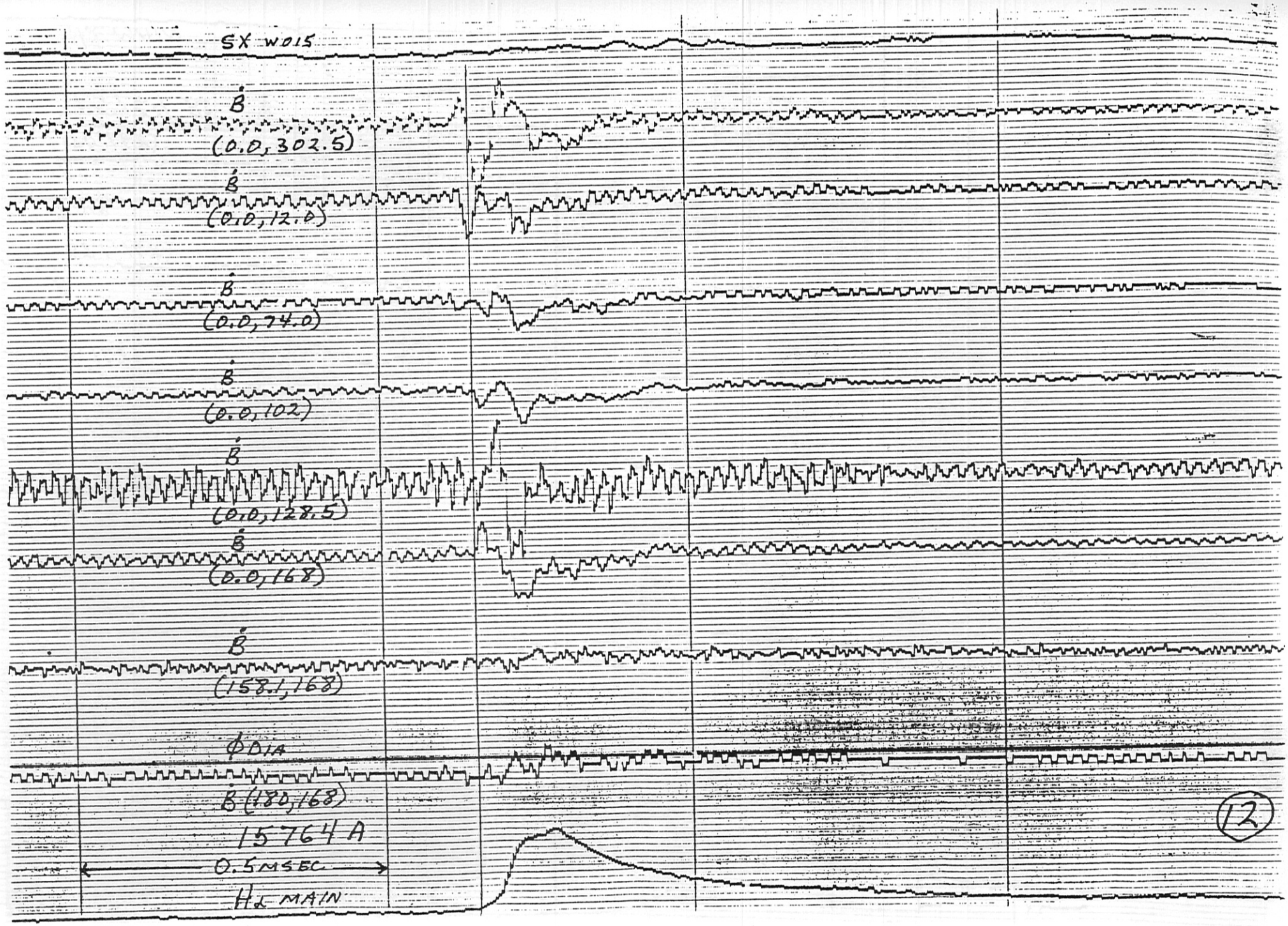
SX W015
$\dot{B}$
(0.0, 302.5)
$\dot{B}$
(0.0, 12.0)
$\dot{B}$
(0.0, 74.0)
$\dot{B}$
(0.0, 102)
$\dot{B}$
(0.0, 128.5)
$\dot{B}$
(0.0, 168)
$\dot{B}$
(158.1, 168)
ϕ DIA
$\dot{B}$ (180, 168)
1576 4 A
0.5 MSEC
H2 MAIN
12

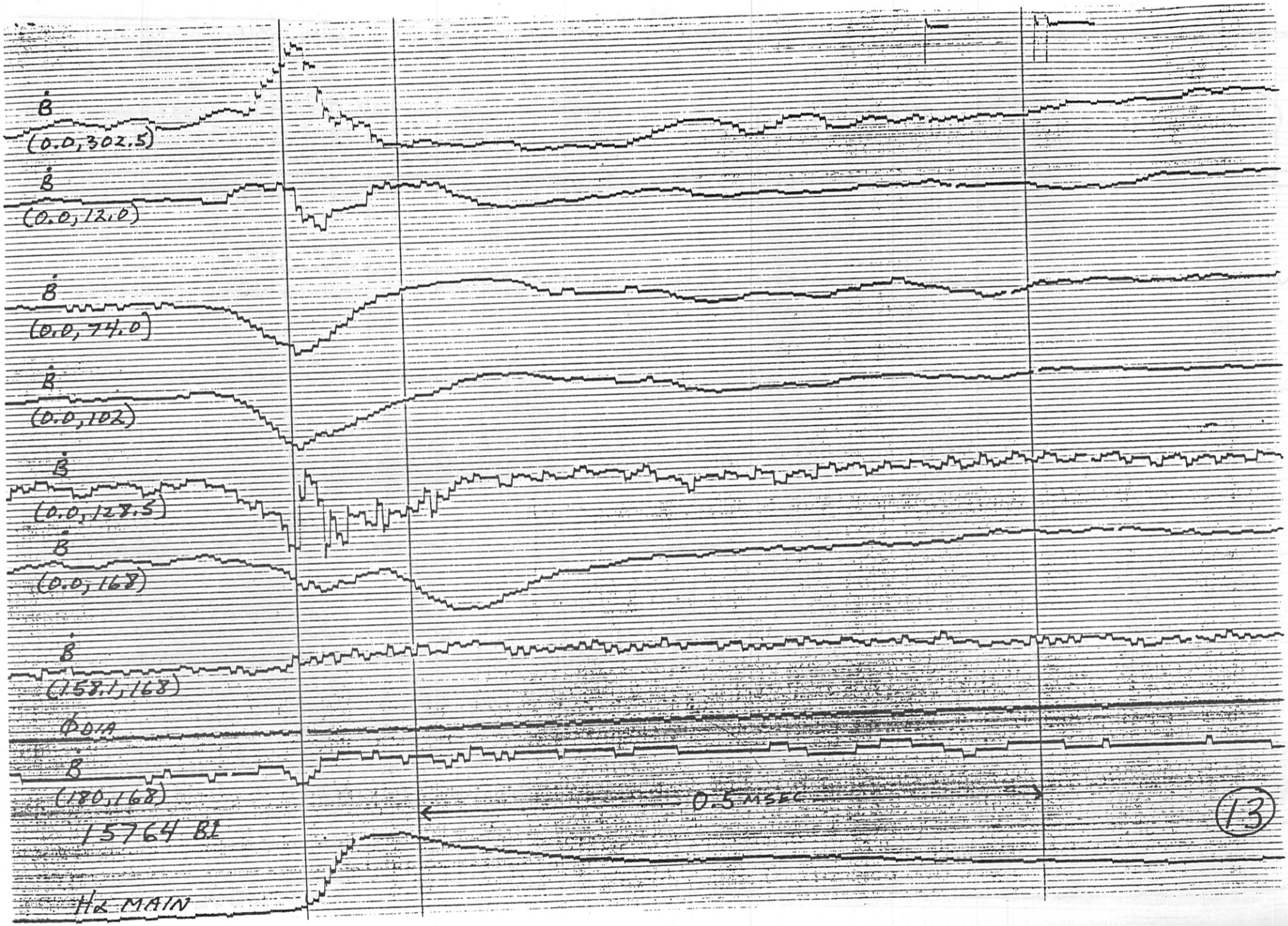
$\dot{B}$
(0.0, 302.5)
$\dot{B}$
(0.0, 12.0)
$\dot{B}$
(0.0, 74.0)
$\dot{B}$
(0.0, 102)
$\dot{B}$
(0.0, 128.5)
$\dot{B}$
(0.0, 168)
$\dot{B}$
(158.1, 168)
Φ_{01A}
$\dot{B}$
(180, 168)
15764 B.I
0.5 MSEC
H.L MAIN
13

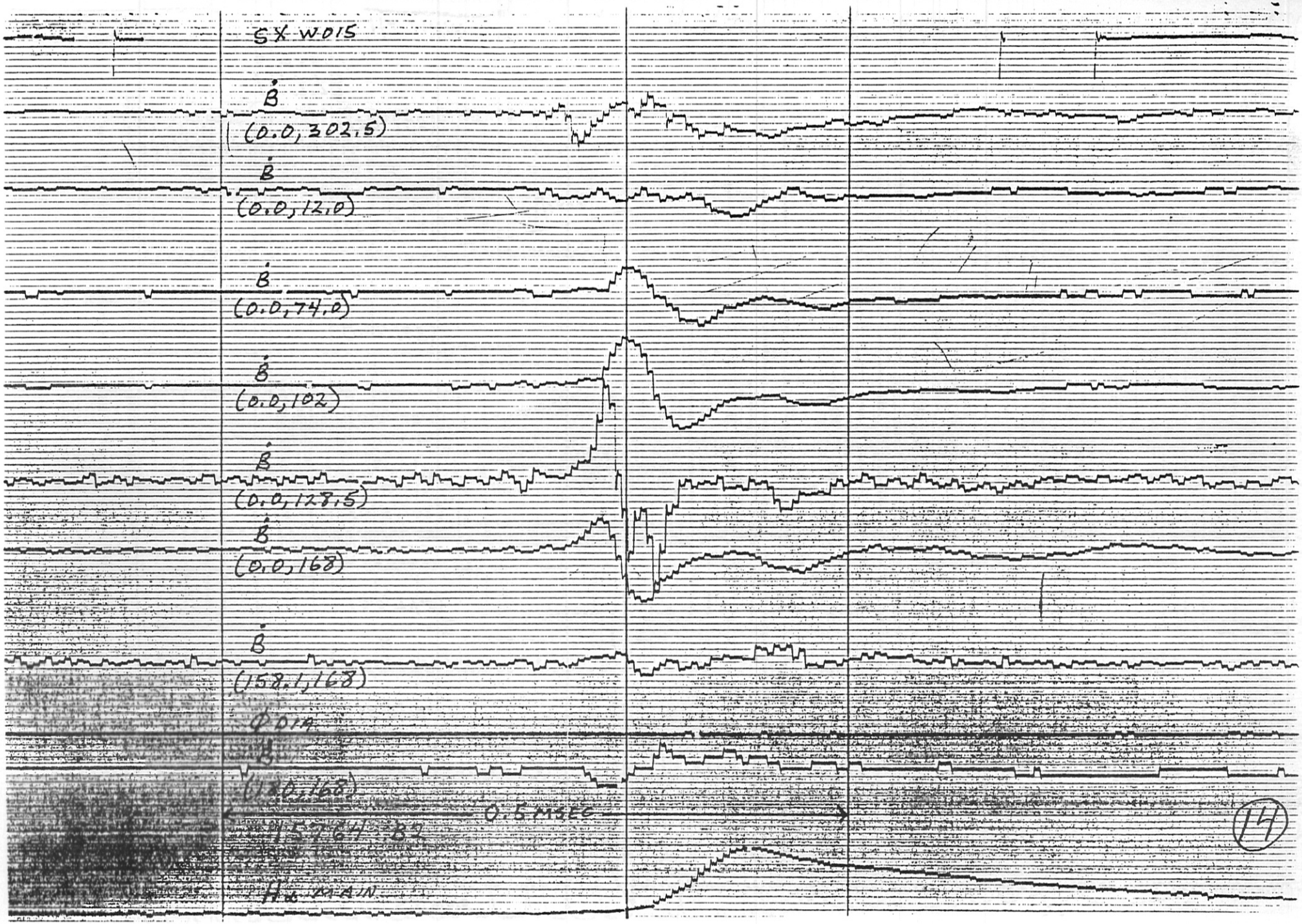
SX WOIS
$\dot{B}$
(0.0, 302.5)
$\dot{B}$
(0.0, 12.0)
$\dot{B}$
(0.0, 74.0)
$\dot{B}$
(0.0, 102)
$\dot{B}$
(0.0, 128.5)
$\dot{B}$
(0.0, 168)
$\dot{B}$
(158.1, 168)
ϕ DIA
$\dot{B}$
(180, 160)
0.5 MSEC
H_ϕ MAIN

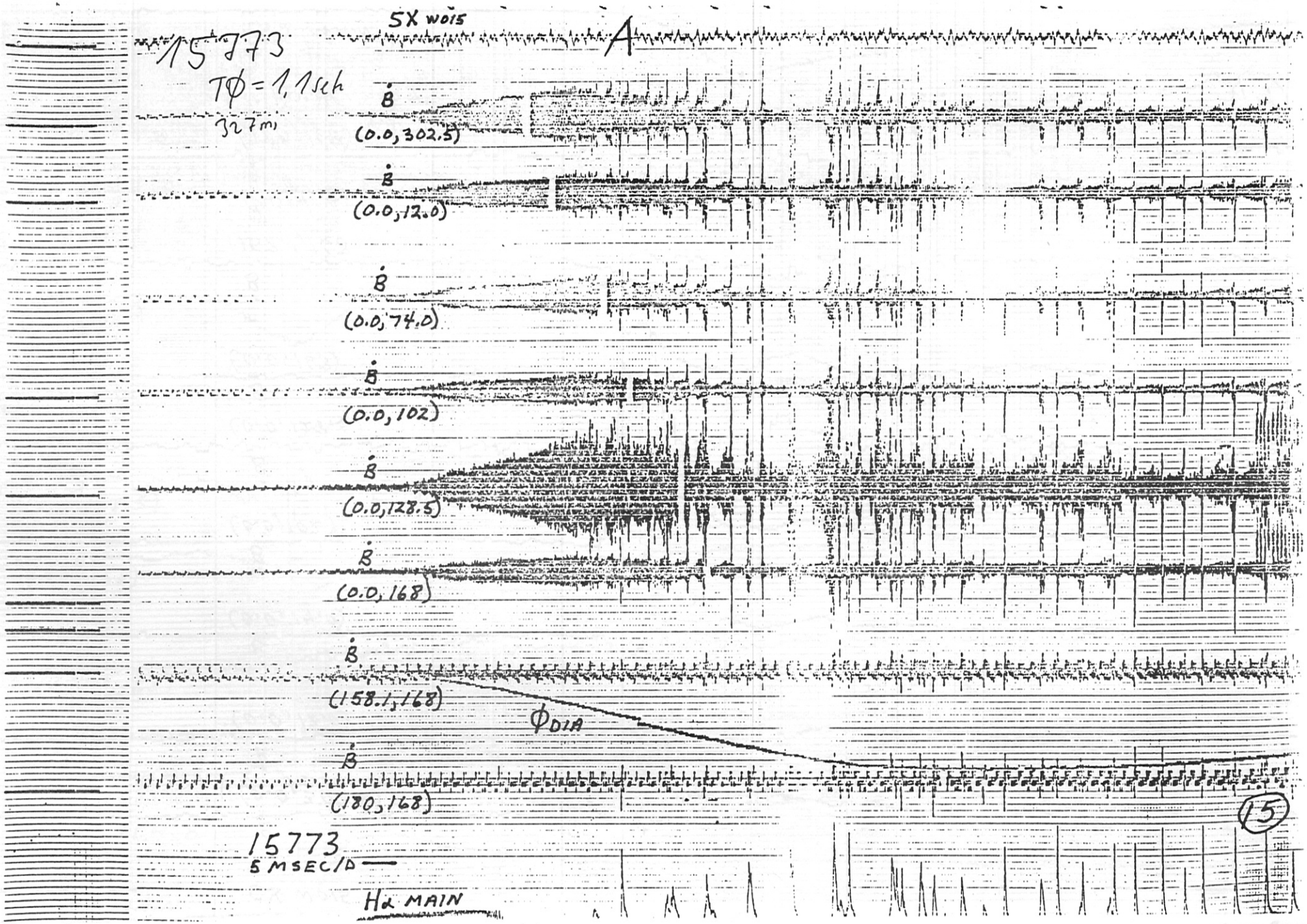
15773
TΦ = 1,1sek
327mi
5X W015
A
Ḃ
(0.0,302.5)
Ḃ
(0.0,12.0)
Ḃ
(0.0,74.0)
Ḃ
(0.0,102)
Ḃ
(0.0,128.5)
Ḃ
(0.0,168)
Ḃ
(158.1,168)
ΦDIA
Ḃ
(180,168)
15
15773
5 MSEC/D
Hz MAIN

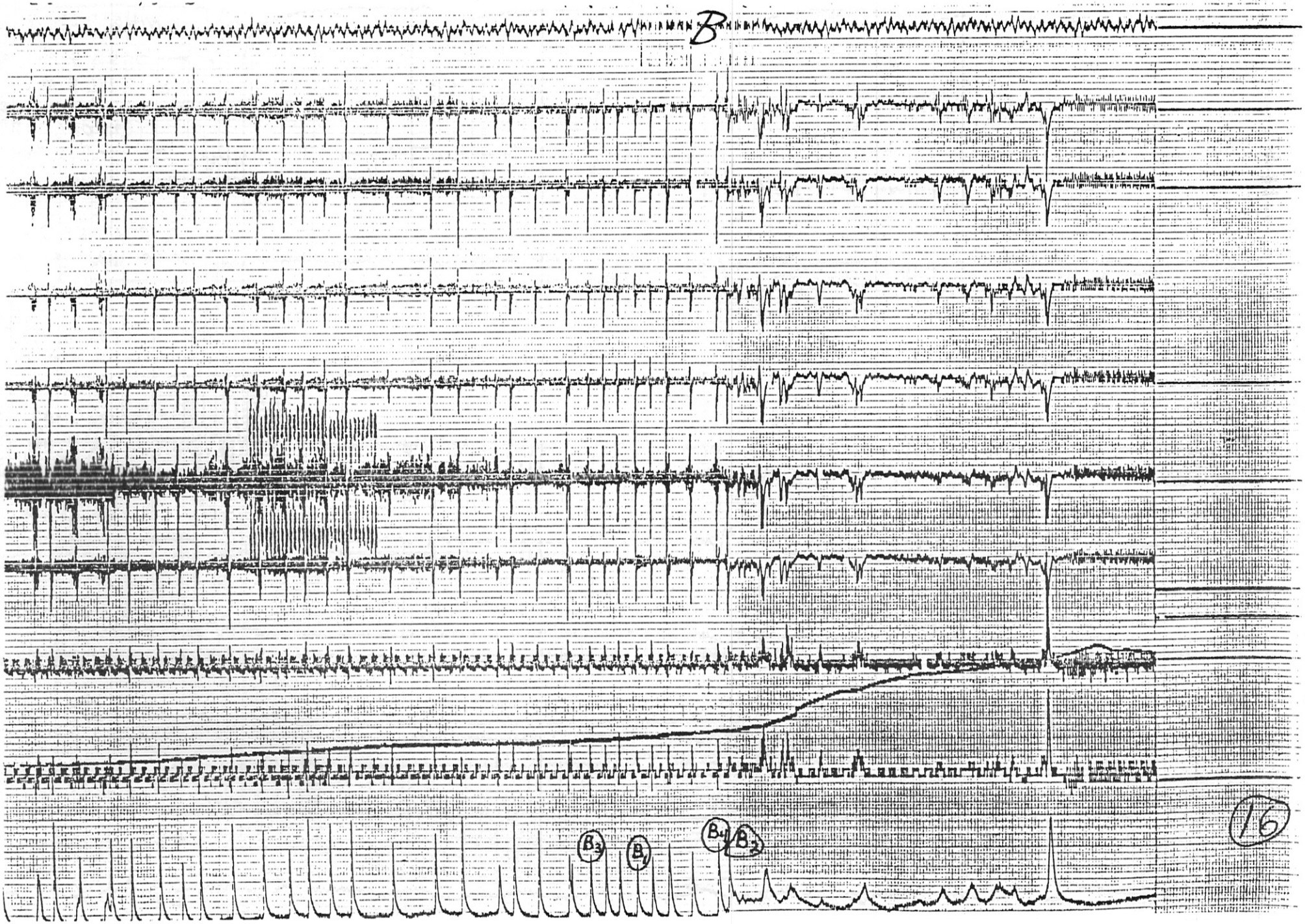
B
B3
B1
B4
B2
16

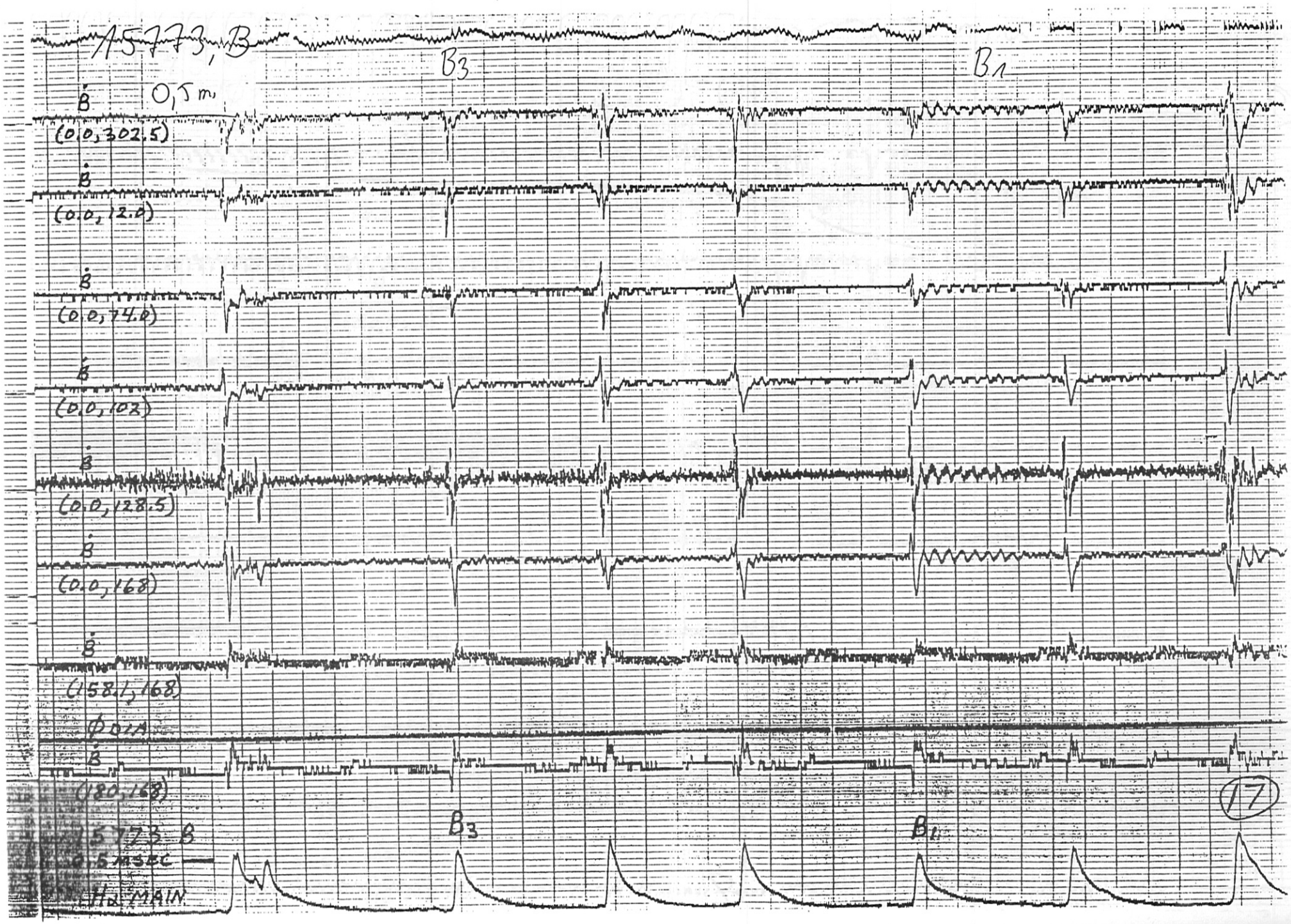
A-5773, B
B3
B1
0,5 m
Ḃ
(0.0, 302.5)
Ḃ
(0.0, 12.0)
Ḃ
(0.0, 74.0)
Ḃ
(0.0, 102)
Ḃ
(0.0, 128.5)
Ḃ
(0.0, 168)
Ḃ
(158.1, 168)
ϕ 01A
Ḃ
(180, 168)
5773 B
0.5 MSEC
H2 MAIN
B3
B1
17

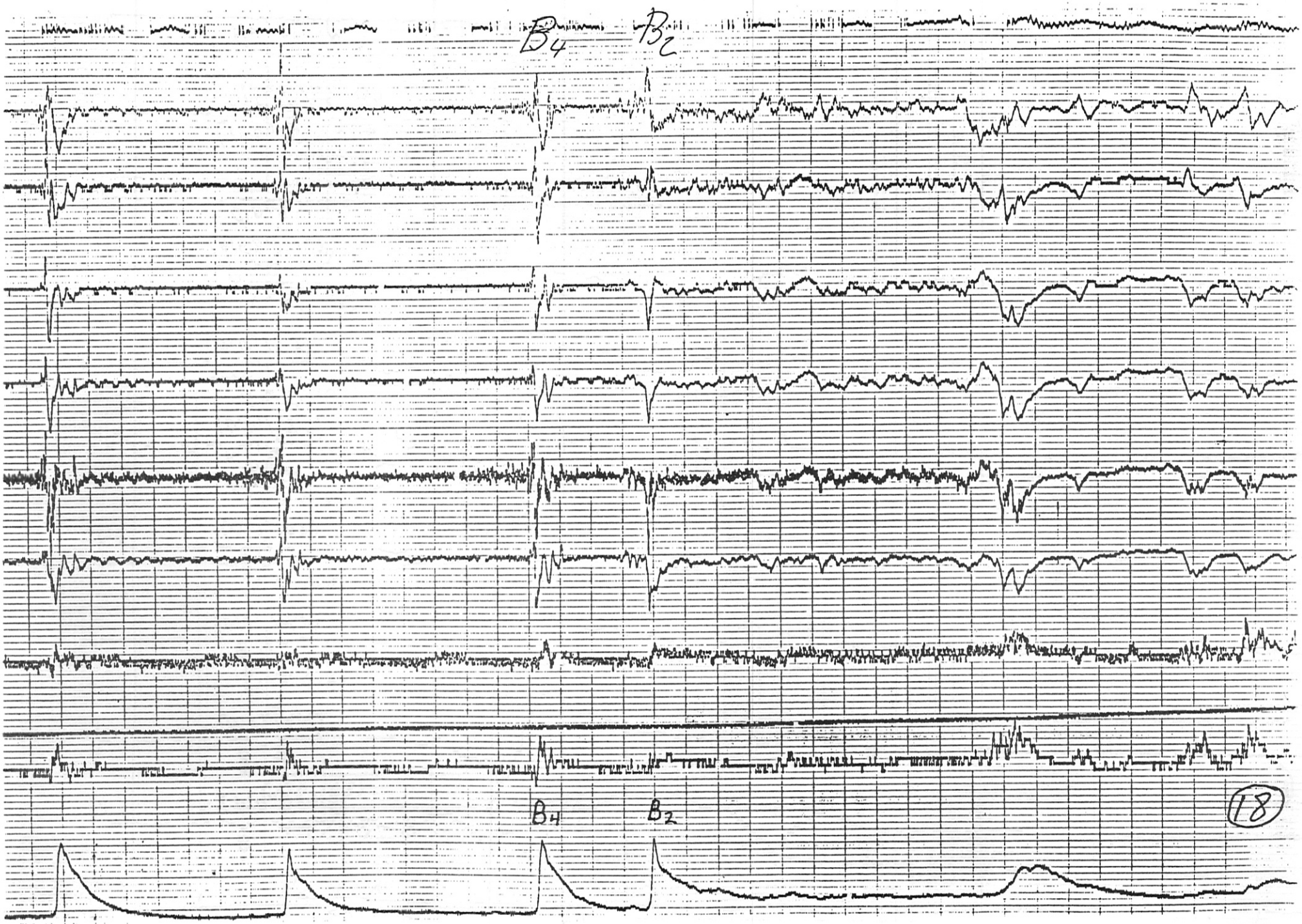
B4
B2
B4
B2
18

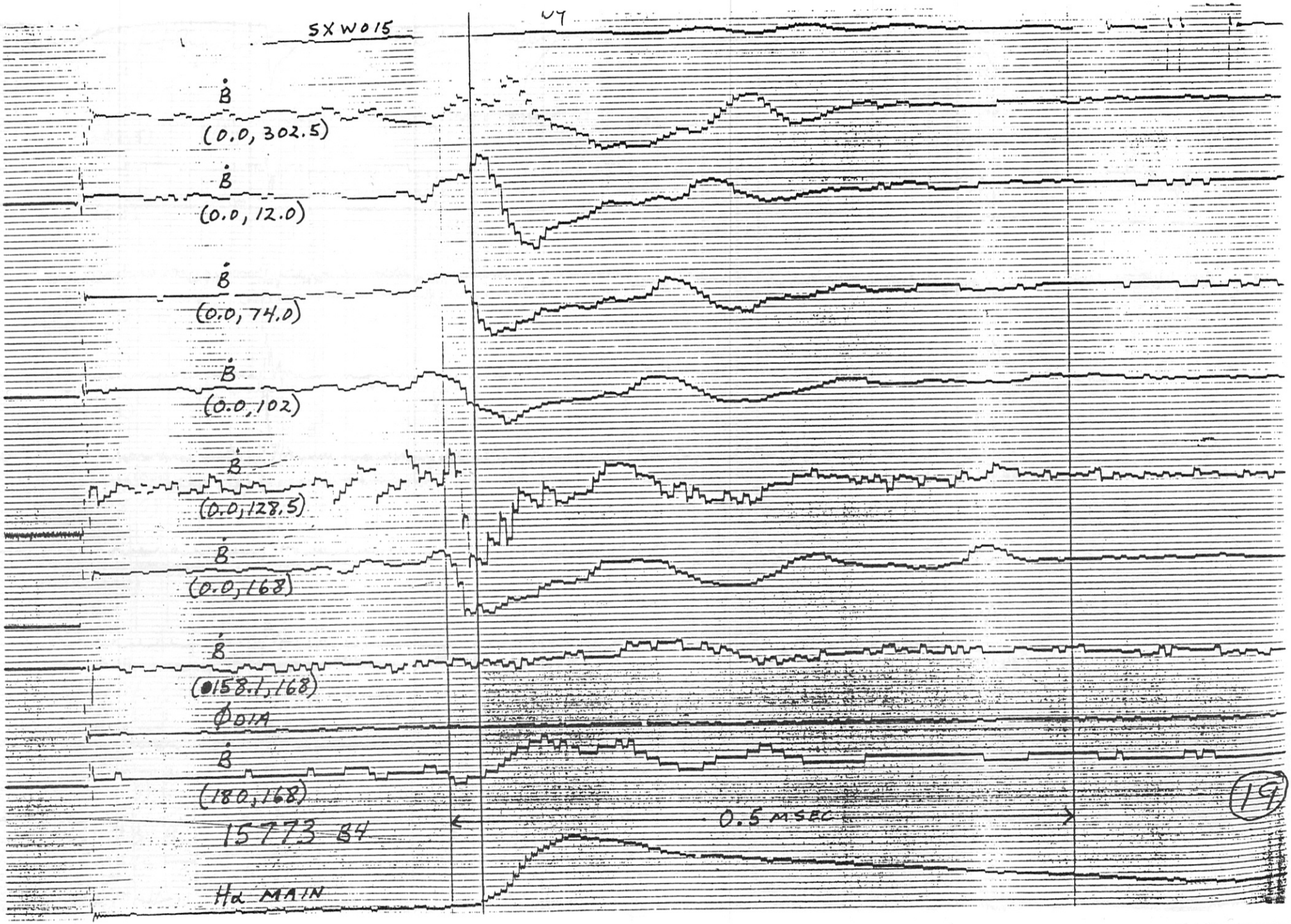
SXW015
$\dot{B}$
(0.0, 302.5)
$\dot{B}$
(0.0, 12.0)
$\dot{B}$
(0.0, 74.0)
$\dot{B}$
(0.0, 102)
$\dot{B}$
(0.0, 128.5)
$\dot{B}$
(0.0, 168)
$\dot{B}$
(158.1, 168)
ϕ_{DIA}
$\dot{B}$
(180, 168)
15773 84
H_α MAIN
0.5 MSEC
19

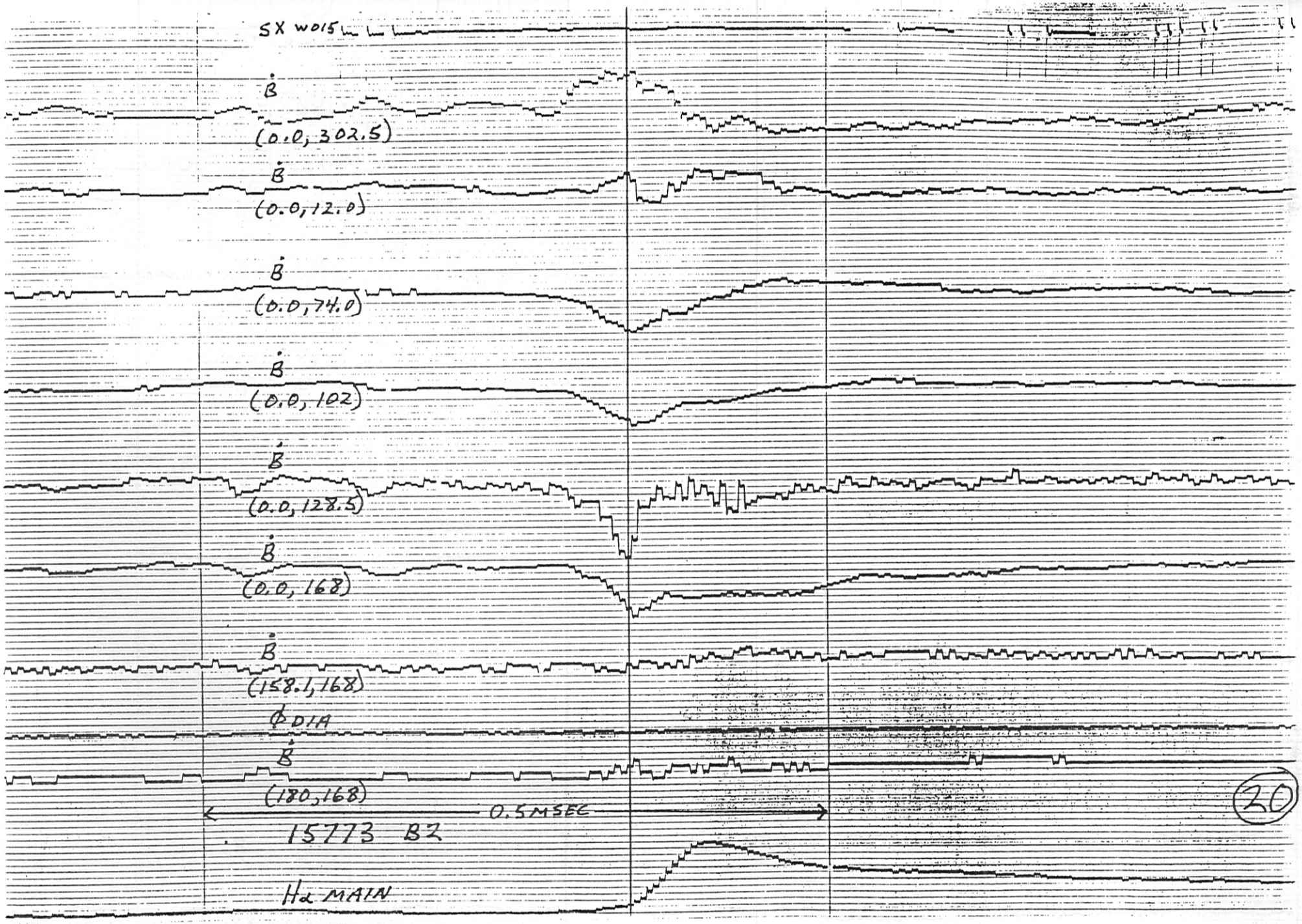
SX W015
$\dot{B}$
(0.0, 302.5)
$\dot{B}$
(0.0, 12.0)
$\dot{B}$
(0.0, 74.0)
$\dot{B}$
(0.0, 102)
$\dot{B}$
(0.0, 128.5)
$\dot{B}$
(0.0, 168)
$\dot{B}$
(158.1, 168)
ϕ DIA
$\dot{B}$
(180, 168)
0.5 MSEC
15773 B2
H$_2$ MAIN
20

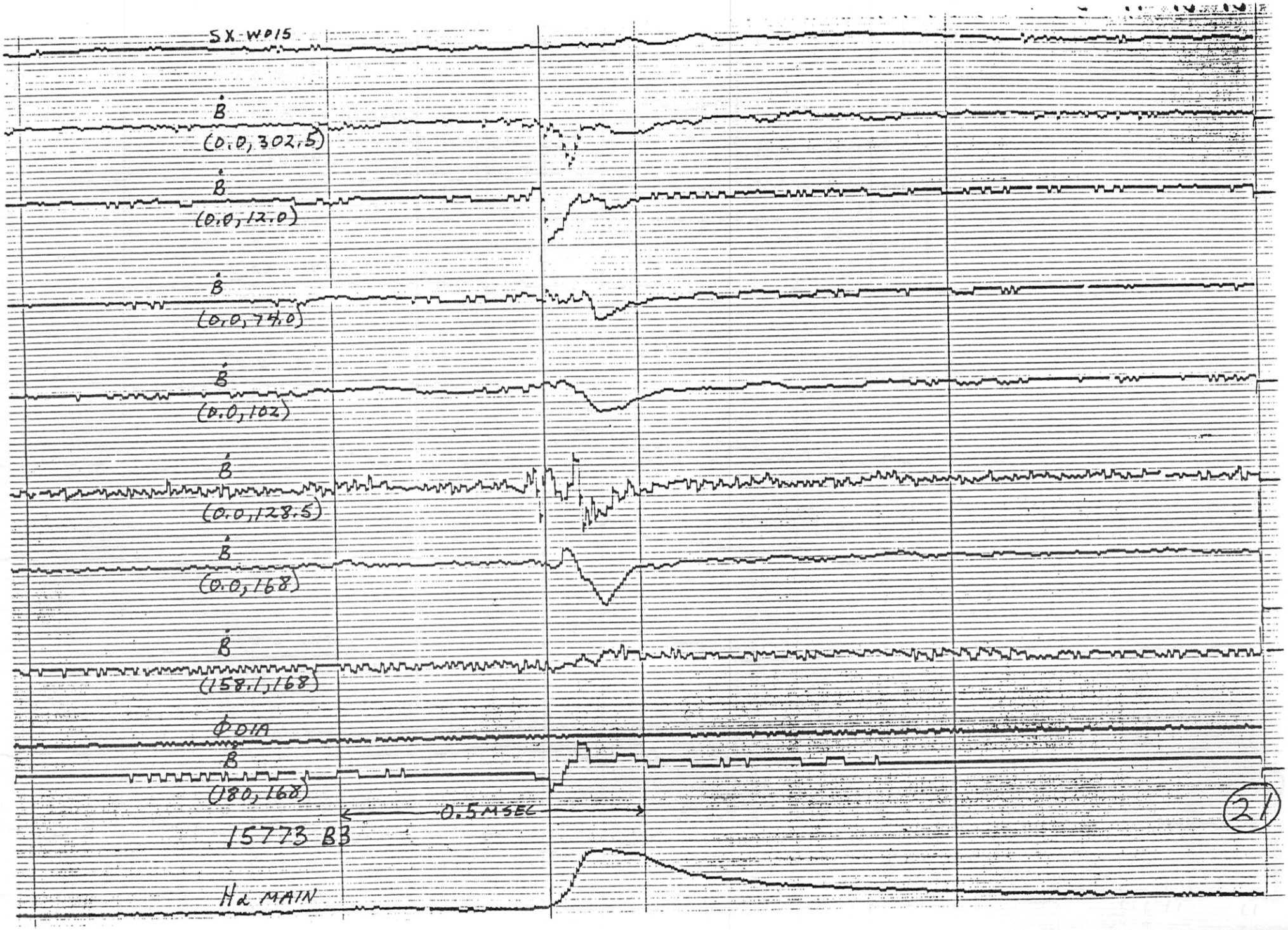
SX-WP15
$\dot{B}$
(0.0, 302.5)
$\dot{B}$
(0.0, 12.0)
$\dot{B}$
(0.0, 74.0)
$\dot{B}$
(0.0, 102)
$\dot{B}$
(0.0, 128.5)
$\dot{B}$
(0.0, 168)
$\dot{B}$
(158.1, 168)
ϕ DIA
B
(180, 168)
0.5 MSEC
15773 BB
H_2 MAIN
21

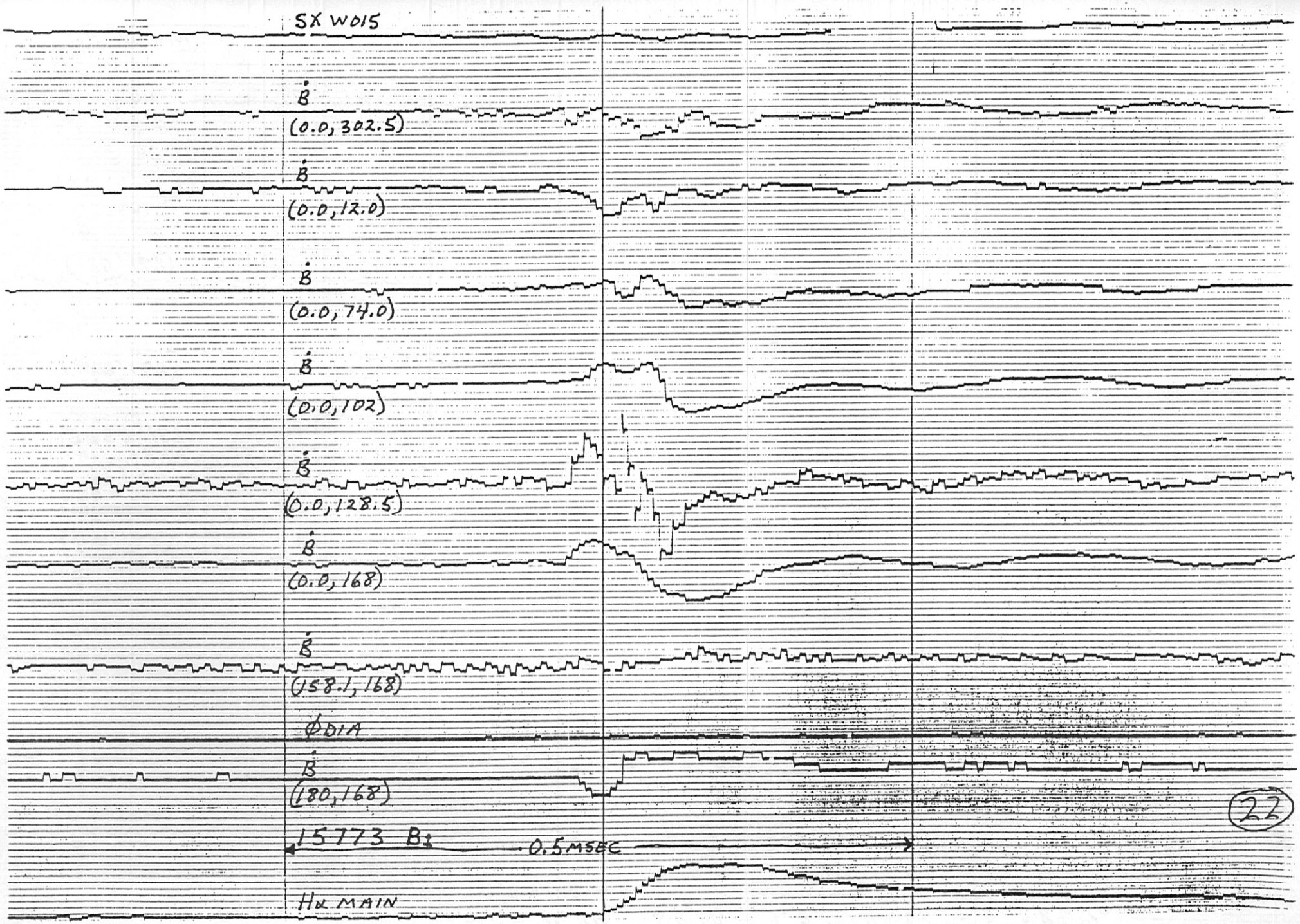
SX W015
$\dot{B}$
(0.0, 302.5)
$\dot{B}$
(0.0, 12.0)
$\dot{B}$
(0.0, 74.0)
$\dot{B}$
(0.0, 102)
$\dot{B}$
(0.0, 128.5)
$\dot{B}$
(0.0, 168)
$\dot{B}$
(158.1, 168)
ϕ_{DIA}
$\dot{B}$
(180, 168)
15773 B_z
0.5 MSEC
H_R MAIN
22

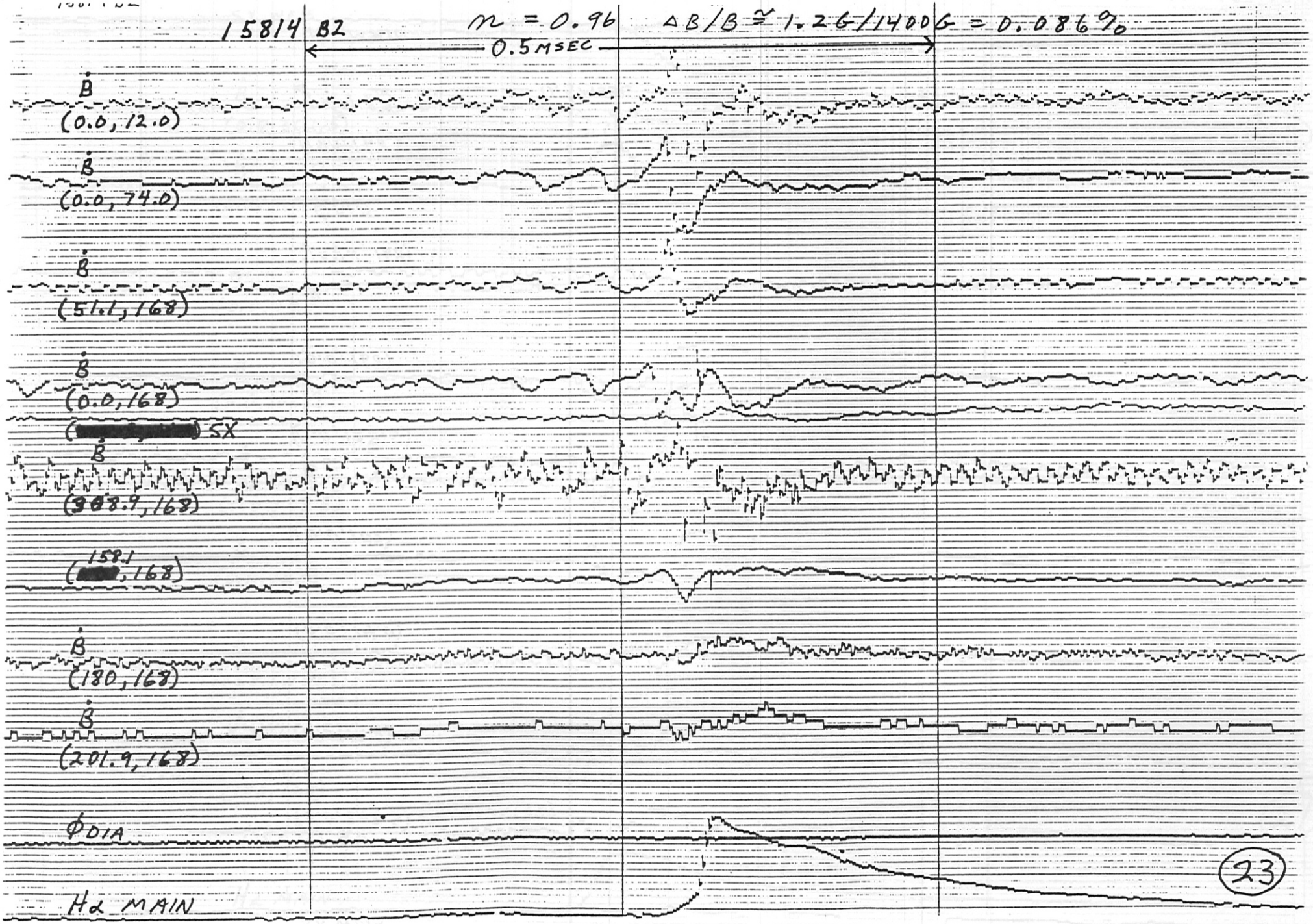
15814 B2
n = 0.96
ΔB/B ≃ 1.26/1400
G = 0.086%
0.5 MSEC
Ḃ (0.0, 12.0)
Ḃ (0.0, 74.0)
Ḃ (51.1, 168)
Ḃ (0.0, 168)
[redacted] SX
Ḃ (308.9, 168)
158.1 [redacted], 168)
Ḃ (180, 168)
Ḃ (201.9, 168)
ΦDIA
H2 MAIN
23